

**Assessing historical variability of South Asian monsoon
lows and depressions with an optimized tracking
algorithm**

S. Vishnu¹, W. R. Boos^{1,2}, P. A. Ullrich³, T. A. O'Brien^{4,2}

¹Department of Earth and Planetary Science, University of California, Berkeley, Berkeley, California, USA

²Climate and Ecosystem Sciences Division, Lawrence Berkeley National Laboratory, Berkeley, California, USA

³Department of Land, Air, and Water Resources, University of California, Davis, Davis, California, USA

⁴Earth and Atmospheric Sciences Department, Indiana University, Bloomington, Indiana, USA

Key Points:

- The streamfunction of the horizontal wind is shown to be highly skillful for identifying monsoon low pressure systems (LPS)
- Uncertainty analyses show that previously reported trends in Indian monsoon depressions may be artifacts of changes in the observing network
- More LPS form in La Niña and wet monsoon years, but other interannual climate modes do not modulate LPS consistently across five reanalyses

17 **Abstract**

18 Cyclonic low-pressure systems (LPS) produce abundant rainfall in South Asia, where
 19 they are traditionally categorized as monsoon lows, monsoon depressions, and more intense
 20 cyclonic storms. The India Meteorological Department (IMD) has tracked monsoon depres-
 21 sions for over a century, finding a large decline in their number in recent decades, but their
 22 methods have changed over time and do not include monsoon lows. This study presents
 23 a fast, objective algorithm for identifying monsoon LPS and uses it to assess interannual
 24 variability and trends in reanalyses. Variables and thresholds used in the algorithm are
 25 selected to best match a subjectively analyzed LPS dataset while minimizing disagreement
 26 between four reanalyses in a training period. The streamfunction of 850 hPa horizontal
 27 wind is found to be optimal in this sense; it is less noisy than vorticity and represents the
 28 complete non-divergent wind, even when flow is not geostrophic. Using this algorithm, LPS
 29 statistics are computed for five reanalyses, and none show a detectable trend in monsoon
 30 depression counts since 1979. Both the Japanese 55-year Reanalysis (JRA-55) and the IMD
 31 dataset show a step-like reduction in depression counts when they began using geostationary
 32 satellite data, in 1979 and 1982 respectively; the 1958–2018 linear trend in JRA-55, how-
 33 ever, is smaller than in the IMD dataset and its error bar includes zero. There are more
 34 LPS in seasons with above-average monsoon rainfall and in La Niña years, but few other
 35 large-scale modes of interannual variability are found to modulate LPS counts, lifetimes, or
 36 track length consistently across reanalyses.

37 **1 Introduction**

38 Cyclonic low pressure systems (LPS) are the dominant synoptic-scale phenomena that
 39 bring rain to India and surrounding regions during the boreal summer monsoon season.
 40 With outer diameters near 2,000 km, these monsoon LPS typically form over the northern
 41 Bay of Bengal then propagate to the northwest over India during the subsequent several
 42 days (Mooley, 1973; Godbole, 1977; Sikka, 1978). Although these storms have weak surface
 43 winds of order 10 m s^{-1} , they produce abundant rainfall, with precipitation rates peaking
 44 at $3\text{-}5 \text{ cm day}^{-1}$ in composite means and some storms producing 10–50 cm of rain along
 45 their tracks (Sanders, 1984; Sikka, 2006; Boos et al., 2015; Hunt et al., 2016). Monsoon LPS
 46 make a large contribution to the total summer monsoon rainfall of continental South Asia
 47 (Yoon & Chen, 2005) and have produced catastrophic floods there (Houze Jr et al., 2011).

48 Given the importance of monsoon LPS, there is great interest in studying the variability
 49 of these storms. The India Meteorological Department (IMD) has kept records on LPS since
 50 the late nineteenth century (India Meteorological Department, 2011). They traditionally
 51 categorized these storms by intensity, with the weakest systems called monsoon lows (surface
 52 wind speeds less than 8.5 m s^{-1} and mean sea level pressure (MSLP) at least 2 hPa lower
 53 than surrounding regions), stronger systems called monsoon depressions (wind speeds $8.5\text{-}13.5 \text{ m s}^{-1}$ and
 54 MSLP anomalies 4–8 hPa), and even stronger vortices called deep depressions
 55 and cyclonic storms (the use of surface wind speed or surface pressure as a metric for
 56 categorization has varied over time (India Meteorological Department, 2011)). The historical
 57 IMD dataset includes only depressions and stronger storms, but Mooley and Shukla (1987)
 58 and Sikka (2006) produced a separate dataset of both lows and depressions by manually
 59 identifying LPS from hand-analyzed daily weather charts of the IMD. These datasets have
 60 been used in numerous studies of variations in the number of monsoon LPS. For example,
 61 the number of LPS forming each summer has been shown to be modulated by the El Niño-
 62 Southern Oscillation (ENSO) (Hunt et al., 2016), the Pacific Decadal Oscillation (PDO)
 63 (Vishnu et al., 2018), and the Indian Ocean Dipole (IOD) (Krishnan et al., 2011), all of
 64 which are also associated with interannual variations in the strength of the mean Indian
 65 summer monsoon.

66 Based on the two track datasets just discussed, numerous studies have reported a large
 67 decrease in the number of monsoon depressions forming each summer in recent decades,

68 together with an increase in the number of monsoon lows (Rajendra Kumar & Dash, 2001;
 69 Prajeesh et al., 2013; Vishnu et al., 2016, and reference therein). When characterized as a
 70 linear trend, the decrease in depression counts amounts to a reduction of around one per
 71 decade, from a mid-twentieth century value of about seven, although much of the decrease
 72 occurred as a step-wise reduction in the early 1980s (Vishnu et al., 2016). The years 2002,
 73 2010, and 2012 contained the first summers, in over a century of record-keeping by IMD,
 74 with no monsoon depressions. The reduction in depression counts has been argued to
 75 be associated with a decrease in total summer rainfall in east-central India, the region
 76 of highest LPS track density (Vishnu et al., 2016). A decrease in overall LPS activity,
 77 including that of both lows and depressions, has been projected for the coming century as
 78 global mean temperature increases and the large-scale, seasonal mean monsoon circulation
 79 weakens (Sandeep et al., 2018; Rastogi et al., 2018). This projected decrease is accompanied
 80 by a poleward shift in the region of LPS genesis in next-century simulations using one global
 81 climate model (Sandeep et al., 2018), but the connection of such greenhouse gas-forced
 82 changes to past trends remains unclear, especially given the possible dominance of aerosol
 83 forcings in historical trends of mean monsoon strength (Ramanathan et al., 2005; Bollasina
 84 & Nigam, 2009).

85 The existence of a large trend in monsoon depression counts was questioned by Cohen
 86 and Boos (2014), who showed that no such trend could be detected in two reanalyses when
 87 automated algorithms were used to track and classify low-level vorticity and MSLP anomalies.
 88 Furthermore, Cohen and Boos (2014) found depression-strength LPS in those reanalyses
 89 during the years when IMD recorded none (2002, 2010 and 2012), and showed that
 90 satellite scatterometer data validated the intensity of the peak surface wind speeds near the
 91 centers of those particular storms. They also showed that there was no detectable trend
 92 in a satellite scatterometer record of synoptic-scale wind events over the Bay of Bengal,
 93 although that record extended back to only 1987. All of this raises numerous questions: are
 94 the two reanalyses examined by Cohen and Boos (2014) reliable tools for assessing trends in
 95 monsoon LPS, especially given that they extended back to only 1979, a few years before the
 96 step-wise reduction in IMD's depression counts? Should we expect trends inferred from the
 97 IMD record of depression counts to be unbiased, given the large changes since the late 19th
 98 century in the observing network, in methods used by IMD for identifying and classifying
 99 LPS, and possibly in practices used for creating the hand-drawn IMD weather charts?

100 All of this would seem to call for a reanalysis of monsoon LPS track datasets, analogous
 101 to the large international efforts to improve track datasets of past tropical cyclones (Landsea
 102 et al., 2008; Hagen et al., 2012; Landsea et al., 2014; Delgado et al., 2018). This would be
 103 a massive undertaking, made more difficult by the fact that IMD synoptic charts are not
 104 readily available and by the fact that monsoon LPS have weak circulations compared to
 105 tropical cyclones. Furthermore, the wind maxima of LPS are typically elevated a few kilo-
 106 meters above the surface (Godbole, 1977), rendering their identification and categorization
 107 using maps of MSLP even more difficult. Here we take an alternate approach by devising
 108 an algorithm that can identify LPS using elevated winds as well as surface conditions as
 109 represented in five atmospheric reanalyses, including the most modern ones that represent
 110 climate forcings and that extend back in time to the 1950s. This does not eliminate bias that
 111 might be introduced by the temporal evolution of the observing network on which those re-
 112 analyses are based, and, indeed, we demonstrate that step-wise changes in depression counts
 113 coincide with dates on which geostationary satellite imagery begin to be incorporated into
 114 the atmospheric state estimates.

115 This study builds on previous attempts to compile LPS track datasets from reanal-
 116 yses (Hurley & Boos, 2015; Praveen et al., 2015), but with greater attention paid to the
 117 optimality of the tracking algorithm, to uncertainty characterization, to separation of the
 118 datasets used for training and validation of the algorithm, and to application of the algo-
 119 rithm to a larger number of reanalyses and to more modern reanalyses. Past efforts to track
 120 LPS in atmospheric reanalyses used the TRACK algorithm (Hodges, 1995, 1998; Hurley

& Boos, 2015), which runs serially and requires degrading the underlying dataset to T42 spectral resolution (Thornicroft & Hodges, 2001; Manganello et al., 2019); both of those characteristics become problematic when working with modern atmospheric state estimates which often have horizontal grid spacings of 20-30 km. The algorithm we create for LPS identification builds on the TempestExtremes software (Ullrich & Zarzycki, 2017) and is thus fast, objective, and appropriate for high-resolution and variable grids. We hope to use this algorithm in future work to track monsoon LPS in large ensembles of high-resolution output from numerical weather prediction models and global climate models. In this study, the main focus is on constructing the algorithm, demonstrating its fidelity compared to existing, subjectively analyzed LPS datasets (Sikka, 2006), then examining the historical variability of LPS tracks on interannual and longer time scales.

2 Data and methods

2.1 Subjectively analyzed track datasets

We use two subjectively analyzed datasets of LPS tracks and intensities in the northern Indian Ocean. The first was compiled by Sikka (2006) and Mooley and Shukla (1987) and runs from 1888-2003, for the months of June through September. We hereafter refer to this as the Sikka archive. As mentioned in the Introduction, the Sikka archive is the only subjectively analyzed track dataset for South Asia that contains both lows and depressions, and it was compiled by manually identifying minima in maps of MSLP from the IMD and then classifying those minima by intensity. The second dataset we use is the total number of depressions forming between June and September from 1891-2019, as recorded by the IMD (<http://www.rmcchennaiatlas.tn.nic.in>). We also use IMD best track data for depressions for 1982-2018.

2.2 Reanalyses

Five global atmospheric reanalyses are used for this study, with horizontal grid spacings ranging from 0.25-1.25° and temporal resolutions ranging from hourly to 6-hourly (Table 1). The variables used are MSLP, surface wind and surface height, and the 850 hPa horizontal wind and relative humidity. All of the reanalyses used here assimilated both satellite and conventional (e.g. surface station and radiosonde) observations that increased in number and type over time, with the greatest growth seen in satellite observations. For example, ERA-Interim, produced by the European Centre for Medium-Range Weather Forecasts (ECMWF), assimilated more than 10^6 daily observations in 1989 and almost 10^7 per day in 2010; the great majority of these, by count, are from satellite, but surface and radiosonde observations from land and ship-based stations are also included, with a reasonable count over South Asia (Dee et al., 2011).

The most recent reanalysis from ECMWF, ERA5, incorporates newly reprocessed observations and input from more recent instruments that were not assimilated into ERA-Interim (Hersbach & Dee, 2016; Hersbach et al., 2019). Similarly, the Modern-Era Retrospective Analysis for Research and Applications, version 2 (MERRA-2) (Gelaro et al., 2017) and the Climate Forecast System Reanalysis (CFSR) (Saha et al., 2010) both assimilate observations not included by their predecessors, with large increases in observation counts in recent decades. In MERRA-2, for example, the number of assimilated aircraft observations increased gradually by a factor of about four from the late 1990s to 2015, eventually becoming the dominant source of direct measurements of upper-level winds, while large step-like increases in the number of assimilated satellite radiances occurred in 2002, 2008, and 2013 (McCarty et al., 2016). Since we are interested in the large changes in monsoon depression counts seen in IMD data in the late 1970s and early 1980s, we also use the Japanese 55-year Reanalysis (JRA-55) (Ebita et al., 2011; Kobayashi et al., 2015) which extends back to 1958. Only conventional observations were assimilated by JRA-55 before 1971, and the greatest increase in the number of assimilated satellite observations occurred after 1979.

Some of the reanalyses we use include time-varying climate forcings that may influence trends in LPS activity. For example, ERA5 incorporates the Coupled Model Intercomparison Project 5 (CMIP5) radiative forcing, accounting in a self-consistent manner for changing greenhouse gases, volcanic eruptions, sea surface temperature (SST), and sea-ice cover (Hersbach & Dee, 2016; Hersbach et al., 2019). This contrasts with ERA-Interim, which imposes a simple linear trend in greenhouse gas concentrations and uses a succession of different SST and sea ice datasets with some temporal discontinuities (Dee et al., 2011). CFSR incorporates time-evolving greenhouse gases, aerosols, and solar variations, while JRA-55 includes time-varying greenhouse gases but a two-dimensional monthly climatology of aerosol optical depth. MERRA-2 uses a sophisticated assimilation of aerosol observations, together with prescribed increases in carbon dioxide.

2.3 Precipitation and SST data

We employ several additional datasets to create indices used in assessing interannual variations of LPS activity. Indian summer rainfall is obtained from the Indian Institute of Tropical Meteorology (IITM; <http://www.tropmet.res.in/Data\%20Archival-51-Page>) and is used to identify pluvial and drought summer monsoon years. The Oceanic Niño Index (ONI) is used as an ENSO indicator, and obtained from the Climate Prediction Center (https://origin.cpc.ncep.noaa.gov/products/analysis_monitoring/ensostuff/ONI_v5.php). Monthly mean SST from the Hadley Centre Global Sea Ice and Sea Surface Temperature version 2 dataset (HadISST2)(Rayner et al., 2003) is used to compute the Indian Ocean Dipole (IOD) index; specifically, we use a normalized index represented by the anomalous SST difference between the western (10°S – 10°N , 50° – 70°E) and eastern (10°S –Equator, 90° – 110°E) Indian Ocean.

Table 1. Details of reanalysis data used in this study.

Dataset	Spatial resolution	Temporal resolution	Period	Source
Era-Interim	$0.75^{\circ} \times 0.75^{\circ}$	6 hour	1979-2018	Dee et al. (2011)
JRA-55	$1.25^{\circ} \times 1.25^{\circ}$	6 hour	1958-2019	Ebita et al. (2011)
CFSR	$0.5^{\circ} \times 0.5^{\circ}$	6 hour	1979-2010	Saha et al. (2010)
MERRA-2	$0.625^{\circ} \times 0.5^{\circ}$	3 hour	1980-2019	Gelaro et al. (2017)
ERA5	$0.25^{\circ} \times 0.25^{\circ}$	1 hour	1979-2019	Hersbach et al. (2019)

2.4 TempestExtremes

An automated Lagrangian pointwise feature tracker, TempestExtremes, is used for extracting LPS track information from the reanalyses (Ullrich & Zarzycki, 2017). TempestExtremes has been used for tracking features including tropical cyclones, extratropical cyclones, and tropical easterly waves (Ullrich & Zarzycki, 2017; Chavas et al., 2017; Zarzycki et al., 2017; Michaelis & Lackmann, 2019). The basic algorithm uses the MapReduce technique, which operates in two stages: first, parallel identification of suitable candidates at each time step through application of thresholds and/or criteria that enforce a closed contour around the candidate points; second, stitching of nearby candidates over successive time steps to develop object tracks, eliminating candidates that do not exhibit behavior consistent with a transiting feature. Here, we use the specific requirement that candidate points must be within 3 degrees of each other on successive time points to be linked. If no points exist within 3 degrees of an existing point in the succeeding 12 hour period, then the track is terminated. Because we use this 12-hour period, rather than the time resolution

208 of the input data, for joining successive points into a track, the stitching process is not
 209 expected to be highly sensitive to the temporal resolution of the input data.

210 The criteria for initial identification of suitable candidates explored in this work require
 211 identifying features that are local minima or maxima, tagging only the strongest candidate
 212 within 5 degrees great-circle distance, and testing for a closed contour in a specified search
 213 variable of specified magnitude and within a specified distance. The closed contour criterion
 214 is assessed via a depth-first search of grid points away from the nodal feature, ensuring
 215 that all possible paths away from the feature reaching the prescribed distance exhibit an
 216 increase (or decrease) in the search variable of sufficient magnitude. One minor additional
 217 modification is made to remove LPS that may appear due to artifacts of the representation
 218 of high orography in reanalyses: we require the maximum surface geopotential within 2°
 219 of the LPS center to be less than $8000 \text{ m}^2\text{s}^{-2}$ for at least 24 cumulative hours of the LPS
 220 track. That is, LPS that spend nearly their entire lifetime over elevated terrain are not
 221 included in our dataset.

222 Features identified using the above procedure are initially classified as LPS. Monsoon
 223 depressions, which are strong LPS, are subsequently classified by requiring a closed contour
 224 magnitude of MSLP that is greater than or equal to 4 hPa and a maximum surface wind speed
 225 within 3° great-circle distance higher than 8.5 m s^{-1} sustained for at least six hours
 226 along the track, similar to the IMD classification of depressions. LPS that do not satisfy
 227 these criteria are categorized as lows.

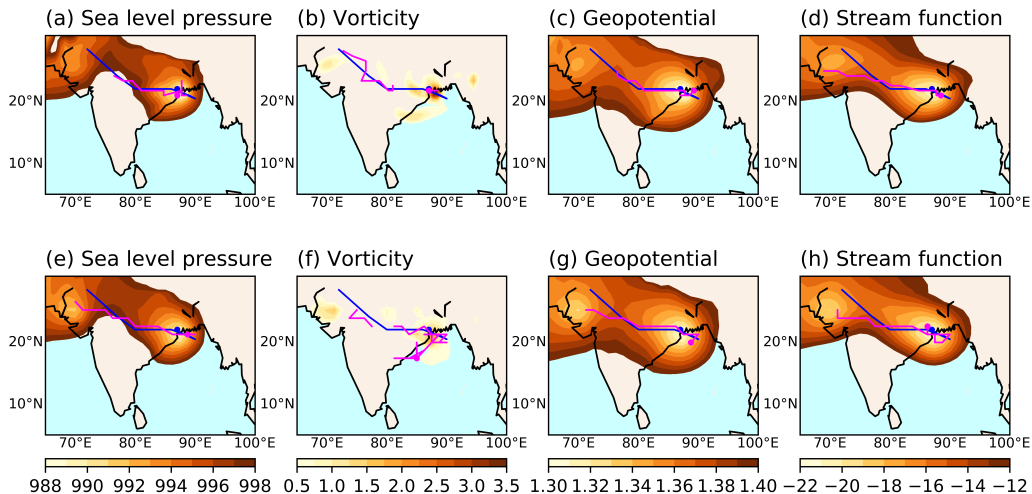


Figure 1. An illustration of LPS tracking using different search variables. The shaded region is (a, e) mean sea level pressure in hPa, (b, f) vorticity at 850 hPa in 10^{-4} s^{-1} , (c, g) geopotential at 850 hPa in $10^4 \text{ m}^2\text{s}^{-2}$ and (d, h) streamfunction at 850 hPa in $10^6 \text{ m}^2\text{s}^{-1}$ on 26–July–2003 00:00 UTC, corresponding to the point of maximum strength during the lifetime of an LPS. The LPS genesis point and track obtained using the given search variable are shown as the magenta dot and line, respectively. The blue dot and line are the Sikka archive LPS genesis point and track, respectively. The top panel shows results from ERA–Interim and the bottom panel from JRA-55.

228 An LPS tracked using four different search variables is shown in Figure 1. The feature
 229 is tracked successfully for all four variables in both ERA-Interim and JRA-55, despite differ-
 230 ences in spatial resolution between these datasets. There are differences in the track length
 231 compared to the Sikka archive. Visually, tracking performed with streamfunction, geopo-
 232 tential, and MSLP matches the Sikka track well, whereas tracking performed using vorticity

233 does not, producing a disjointed track in both reanalyses. We systematically evaluate the
 234 performance of different tracking variables in Section 3.

235 2.5 Skill metric

236 To assess the agreement between LPS tracks obtained from our training datasets (the
 237 reanalyses) and the reference dataset (the Sikka archive), an event-matching algorithm is
 238 employed. Tracks are considered matched between two or more datasets when their points
 239 lie within 3° great-circle distance of each other for at least one day in their lifetime. The
 240 degree of match between tracks in the training and reference datasets is first quantified in
 241 terms of a hit ratio and false alarm ratio. The hit ratio is the fraction of matches in the
 242 reference dataset also detected in a training dataset. The false alarm ratio is the fraction of
 243 features in a training dataset without a match in the reference dataset.

244 We also use the Critical Success Index (CSI) (Di Luca et al., 2015) to assess algorithm
 245 skill. This index accounts for both matches and non-matches using a single skill score,

$$\text{CSI}(\text{dataset, reference}) = \frac{\langle \text{matches} \rangle}{\langle \text{matches} \rangle + \langle \text{non-matches} \rangle}. \quad (1)$$

246 Here $\langle \text{matches} \rangle$ is the count of matches between a training dataset and the reference dataset,
 247 and $\langle \text{non-matches} \rangle$ is the average count of non-matches in the training and reference datasets.

248 Since the reference dataset (the Sikka archive) may contain errors, it is inadequate
 249 to simply choose a tracking algorithm that maximizes the CSI for this single reference
 250 dataset. Hence, we also consider the degree to which a track is represented similarly across all
 251 reanalyses. We create a combined CSI that weights agreement between all of the reanalyses
 252 with agreement between the reanalyses and the Sikka archive,

$$\text{CSI}_{\text{combined}} = \frac{\text{CSI}_{EJCM} + \frac{\text{CSI}_{ES} + \text{CSI}_{JS} + \text{CSI}_{CS} + \text{CSI}_{MS}}{4}}{2}. \quad (2)$$

253 Here CSI_{EJCM} is the CSI among all four reanalyses—namely, considering $\langle \text{matches} \rangle$ to be
 254 the count of LPS common in all four reanalyses and $\langle \text{non-matches} \rangle$ to be the average of non-
 255 matches among all four reanalyses. In the latter case, we define a non-match as occurring in
 256 a particular reanalysis when the LPS detected in that reanalysis is not identified in at least
 257 one other reanalysis. The terms CSI_{ES} , CSI_{JS} , CSI_{CS} and CSI_{MS} are the four CSI values of
 258 the four individual reanalyses (ERA-Interim, JRA-55, CFSR, and MERRA-2, respectively)
 259 compared with the Sikka archive. The combined CSI is employed to rank the performance
 260 of each tracking algorithm.

261 3 An optimized tracking algorithm

262 Since monsoon lows and depressions have weaker intensities than classic tropical cy-
 263 clones, it has been a challenge to detect and classify these LPS in reanalyses. A variety
 264 of methods have been used for this task, with relatively low levels of agreement between
 265 the resulting track datasets. For example, Hurley and Boos (2015) and Hunt et al. (2016)
 266 both identified LPS as cyclonic extrema of lower tropospheric relative vorticity having con-
 267 current negative anomalies of MSLP relative to a 21-day mean. Those studies used only
 268 ERA-Interim data. Praveen et al. (2015) identified LPS in both ERA-Interim and MERRA
 269 with a detection algorithm designed to mimic the manual identification of LPS performed by
 270 IMD, thus using only MSLP. Even when mimicking the traditional detection methodology,
 271 Praveen et al. (2015) obtained only modest correspondence with the Sikka archive: corre-
 272 lation coefficients for interannual variations of monsoon LPS counts were 0.4 and 0.5 for
 273 ERA-Interim and MERRA, respectively, referenced to the Sikka archive. All of the above
 274 studies chose thresholds (e.g. a 2 hPa MSLP anomaly) for their detection algorithms based
 275 on some combination of physical understanding and traditional identification methods, with
 276 little systematic assessment of those thresholds.

277 3.1 Candidate variables and thresholds

278 Here we assess multiple candidate variables and detection thresholds to obtain a tracking
 279 algorithm that is more nearly optimal across multiple reanalyses. Although it is possible
 280 that every reanalysis and every particular configuration of an atmospheric model will have a
 281 unique geophysical variable and set of thresholds that allow LPS identification to best match
 282 traditional methods (e.g. those used by IMD), retuning tracking algorithms in this way is
 283 undesirable from the perspectives of both practicality and scientific understanding. So we
 284 perform a sensitivity analysis using a set of candidate variables, with ranges of corresponding
 285 thresholds and the skill metric defined above (the CSI).

286 We include MSLP and the 850 hPa relative vorticity (ζ) in this set of candidate variables
 287 because these have previously been used for tracking monsoon LPS and, more generally,
 288 tropical cyclones (for a relevant history see Bengtsson et al. (1982), Broccoli and Manabe
 289 (1990), and Appendix B of Ullrich and Zarzycki (2017)). Drawbacks exist for both of
 290 those variables, with peak values of vorticity depending on the horizontal resolution of the
 291 underlying dataset, and MSLP being only an indirect indicator of the circulation several
 292 kilometers above the surface, where monsoon LPS typically have strongest winds. For this
 293 reason, we also consider the 850 hPa geopotential, which provides the geostrophic circulation
 294 closer to the level of strongest winds. Additionally, we consider the streamfunction (ψ)
 295 of the horizontal wind; through the relation $\nabla^2\psi = \zeta$, it has an exact relation to the
 296 relative vorticity but is much smoother than that variable. The geopotential and MSLP are
 297 similarly related to the vorticity only under conditions of low Rossby number, and monsoon
 298 depressions can easily achieve Rossby numbers of 2 (Boos et al., 2015). A practical challenge
 299 exists when computing ψ on a level of a vertical coordinate system that intersects the ground,
 300 because boundary conditions must be imposed on that intersection when inverting the winds
 301 (or vorticity) to obtain the streamfunction. Some reanalyses (e.g. ERA-Interim) extrapolate
 302 winds beneath Earth's surface, and we choose to replace those extrapolated values with
 303 zero prior to inverting ζ to obtain ψ . More discussion of issues involved in calculating the
 304 streamfunction is provided in Appendix A. In summary, the set of variables used to create
 305 candidate tracking algorithms are MSLP, 850 hPa relative vorticity, 850 hPa geopotential,
 306 and 850 hPa streamfunction (see also Table 2). We later test the sensitivity of the chosen
 307 geophysical variable to the choice of vertical level.

308 Detection of LPS involves using TempestExtremes to locate minima of MSLP, geopo-
 309 tential, or streamfunction, or maxima of vorticity, then testing whether that extremum is
 310 surrounded by a closed contour of the same field within a specified radius. This effectively
 311 tests the magnitude of the radial gradient, relative to a local extremum, in a given variable,
 312 making the algorithm insensitive to trends in the horizontal mean of that variable. Use of
 313 the closed contour criterion reduces the sensitivity of the method to resolution and further-
 314 more resembles traditional methods, as discussed above. See Ullrich and Zarzycki (2017)
 315 for details on how TempestExtremes implements the closed contour criterion. We test eight
 316 closed contour magnitudes and two radii for identifying extrema, with the closed contour
 317 magnitudes and radius together essentially specifying a minimum radial gradient that must
 318 exist for the extremum to be classified as an LPS. We use radii of 5° and 10° of great circle
 319 distance, with the eight closed contour magnitudes for each candidate variable shown in
 320 Table 2. This approach is analogous that used by Zarzycki and Ullrich (2017) in developing
 321 optimal criteria for identification of tropical cyclones using TempestExtremes.

322 We additionally desire a criterion for distinguishing LPS from “heat lows”, which are
 323 non-precipitating low pressure systems trapped in the lower troposphere (Ramage, 1971;
 324 Rácz & Smith, 1999). Heat lows frequently form over northwestern India during summer
 325 and over central India before monsoon onset there; they fulfill all the traditional kinematic
 326 criteria for LPS discussed in the Introduction, but seem to be traditionally excluded from
 327 LPS datasets by some implicit criteria that we suspect involves their geographic location or
 328 moisture content. We initially attempted to use a precipitable water criterion to distinguish
 329 heat lows from traditional LPS, but recognized that the increase in precipitable water ex-

Table 2. Variables and closed contour magnitudes used for detecting low pressure systems.

Search variable	Closed contour magnitudes
Mean sea level pressure (Pa)	25, 50, 75, 100, 125, 150, 175, 200
Geopotential at 850 hPa (m^2s^{-2})	25, 50, 75, 100, 125, 150, 175, 200
Streamfunction at 850 hPa ($10^5 \text{ m}^2\text{s}^{-1}$)	5.0, 7.5, 10.0, 12.5, 15.0, 17.5, 20.0, 25.0
Relative Vorticity at 850 hPa (10^{-5} s^{-1})	2.5, 3.0, 3.5, 4.0, 4.5, 5.0, 5.5, 6.0

pected in a warming climate might create spurious trends in LPS counts. One alternative would be to require a minimum precipitation rate to distinguish heat lows from LPS, motivated by the fact that most interest in LPS exists because of their heavy precipitation. But precipitation rates have large variance on short time and space scales, and are also subject to trends in a warming climate. So we opt to distinguish LPS from heat lows using the 850 hPa relative humidity (RH), averaged within 3° of the LPS center. Eight RH thresholds ranging from 55% to 90%, with an interval of 5%, are used in the candidate tracking algorithms. The RH is required to exceed these thresholds for a cumulative period of at least one day over the disturbance lifetime to be considered an LPS, otherwise it is categorized as a heat low. This choice thus includes systems in our LPS dataset that spend much of their lifetimes as non-precipitating, low-RH disturbances but that achieve high lower-tropospheric RH for at least one day.

3.2 Assessing candidate tracking schemes

Using the above sets of candidate variables, closed contour magnitudes, radii, and RH criteria, we use TemepstExtremes to identify LPS in four reanalyses (ERA-Interim, JRA-55, CFSR, and MERRA-2; see Table 1) for the training period of 1990–2003. This 14-year training period is chosen to overlap with the Sikka archive, which ends in 2003, while leaving a substantial period for verification (1979–1989). A total of 2,048 track datasets are thus created (4 reanalyses \times 4 candidate variables \times 8 closed contour magnitudes \times 2 radii \times 8 RH thresholds). The maximum surface wind speed within 3° of the center is used as the maximum sustained surface wind speed of a storm at a time step, and is used later to classify disturbances as lows and depressions. The land-sea ratio of the grid point at the center of each LPS is used for region-wise categorization, with storms treated as being over land when this ratio is higher than 0.5. The TempestExtremes commands for tracking LPS using these criteria is provided in Appendix B.

We perform a sensitivity analysis by ranking the 512 tracking algorithms, for each of the four reanalyses, by the combined CSI (Figure 2). As described in the previous section, the combined CSI is a weighted average of the agreement of each reanalysis track dataset with the Sikka archive and the agreement between all reanalyses. The top 31 algorithms by this ranking all use the 850 hPa streamfunction. The top-ranked algorithm requires a disturbance to have an 850 hPa streamfunction that increases by 1.25×10^6 from the center minimum within a radius of 10° , while achieving an 850 hPa RH of at least 85% for at least one day. The second-best variable for tracking LPS is the 850 hPa geopotential (closed contour magnitude of $125 \text{ m}^2 \text{ s}^{-2}$ and RH higher than 85%). The lower ranking (32 out of 512) of the geopotential comes mainly from greater disagreement between reanalysis tracks, i.e. a smaller value of CSI_{EJCM} in Equation 2, and algorithms based on geopotential are only slightly less skillful than those based on streamfunction (Figure 2). Since streamfunction is not included in most reanalyses and must be computed prior to running the tracking algorithm, the geopotential is a viable alternative for LPS tracking that requires only a slight compromise in skill. Algorithms based on MSLP have lower skill, with the highest rank of 133 (out of 512); the lower rank comes mainly from greater disagreement between reanalyses but with some contribution from disagreement with the Sikka archive (not shown). The

least skillful algorithms all use the 850 hPa vorticity, with the highest rank of 359 out of 512. The vorticity-based algorithms produce track datasets that disagree most strongly between reanalyses and that differ most with the Sikka archive. This is notable given the number of past studies that have used vorticity or potential vorticity to track synoptic-scale monsoon disturbances in Asia, Africa, and Australia (Hurley & Boos, 2015; Hunt et al., 2016; Thorncroft & Hodges, 2001; Berry et al., 2012). Variables and thresholds for the top-five ranked algorithm and top algorithm of each searching variable are depicted in Table S1.

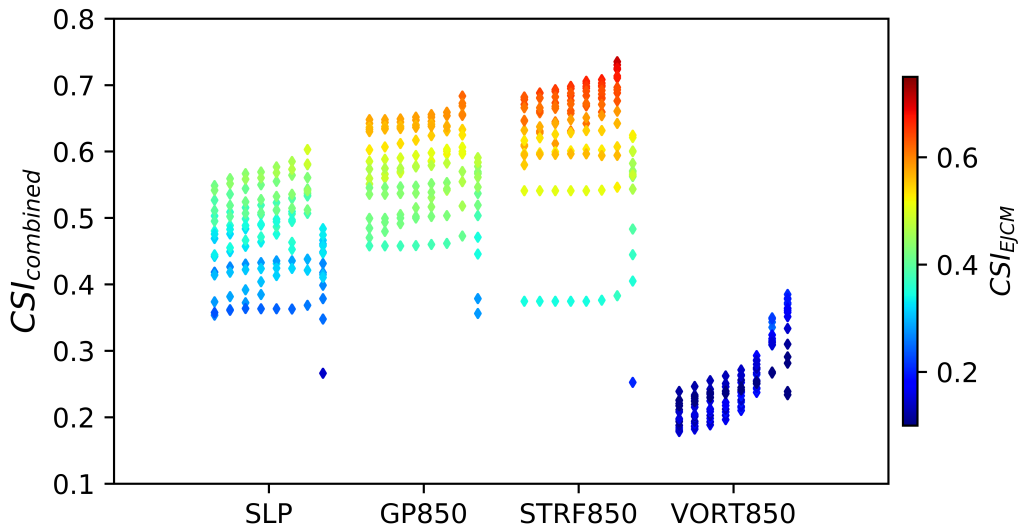


Figure 2. Illustration of the greater skill of 850 hPa streamfunction in detecting LPS. Each diamond marks the combined Critical Success Index (defined in text) for one combination of closed contour magnitude, radius, and RH threshold. Shading represents consistency of the algorithm across reanalyses. The tested variables were mean sea level pressure (SLP), 850 hPa geopotential (GP850), streamfunction of the 850 hPa horizontal wind (STRF850), and 850 hPa relative vorticity (VORT850). Each column within a variable represents one RH threshold, from 55% (left) to 90% (right) with an interval of 5%.

Although the consistency of an algorithm across reanalyses constitutes a large part of its skill score, the top-ranking algorithm also captures more than 80% of LPS in the Sikka archive, our reference dataset. The fraction of LPS in the Sikka archive that are detected in reanalyses (the hit ratio) is plotted against the fraction of LPS detected in reanalyses that do not exist in the Sikka archive (the false alarm ratio) in Figure 3. Tracking algorithms using the 850 hPa streamfunction and 850 hPa geopotential have higher CSI values with higher hit ratios and lower false alarm ratios in all reanalyses. In most reanalyses, algorithms based on MSLP have smaller hit ratios than those based on streamfunction or geopotential. Vorticity-based algorithms have lower CSI values mainly due to higher false alarm ratios in all reanalyses. The top-ranked algorithm by the combined CSI (marked by black circles in Figure 3) compares well with the Sikka dataset in all reanalyses, with hit ratios of about 0.8 and false alarm ratios around 0.3.

We also compute the skill scores outside the training period (in the validation period of 1979–1989), finding that there is little change in the level of agreement between each reanalysis and the Sikka archive; the CSI of ERA-Interim, JRA-55, CFSR and MERRA-2 are 0.79, 0.80, 0.79 and 0.71, respectively, in the training period and 0.78, 0.78, 0.77 and

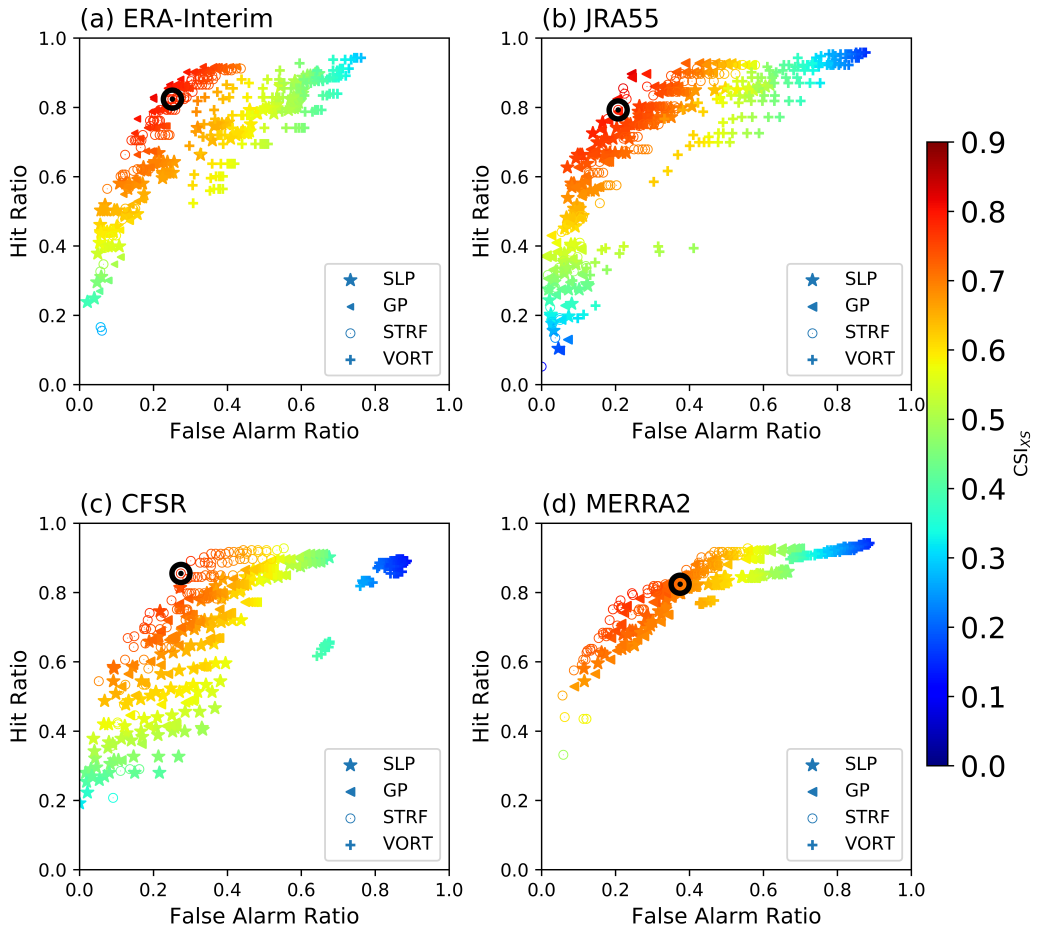


Figure 3. Hit ratio vs. false alarm ratio (see text for definition) with respect to the Sikka archive for all LPS algorithms, shaded by CSI_{XS} for: (a) ERA-Interim, (b) JRA-55, (c) CFSR, and (d) MERRA-2. The black circle represents the selected optimal algorithm (top-ranked by the combined CSI).

0.72, respectively, in the validation period. Remarkably, ERA5, which was not used for training, has a higher CSI (0.83), a higher hit ratio, and a lower false alarm ratio than the other reanalyses. This is true despite the fact that ERA5 has hourly, 0.27° resolution while the reanalyses used for algorithm training have grid spacings coarser by factors of 2-6.

For completeness, we also checked whether combining MSLP and 850 hPa vorticity might improve the tracking algorithm, since previous studies used such combinations of variables (Hurley & Boos, 2015; Hunt et al., 2016). Algorithms using a combination of MSLP and vorticity had CSI values around 0.6, similar to those based on MSLP alone. Furthermore, combining streamfunction and vorticity did not noticeably improve the skill scores. Finally, we tested whether the skill score would improve by using a variable from a different vertical level. Using the streamfunction of horizontal wind at 1000 hPa, 700 hPa, and 500 hPa yielded CSI values lower than those obtained for the 850 hPa streamfunction.

Using the top-ranked algorithm, we track LPS in all available years of all reanalyses (Table 1). This includes ERA5, which was not used for training.

410 **3.3 Are non-matches real systems?**

411 We now check whether the “false alarms”—LPS identified in reanalyses by our top-
 412 ranking algorithm but missing in the Sikka archive—exist due to some error or artifact in
 413 the tracking algorithm. We do this by comparing composites of the structures of reanalysis
 414 LPS that match those in the Sikka archive with composites of those missing from the
 415 Sikka archive. We do this separately for monsoon lows and monsoon depressions, since the
 416 implications of a false alarm are different when the LPS is a weak LPS compared to a strong
 417 one. We furthermore only include a reanalysis LPS in our composites of false alarms when it
 418 is completely missing from the Sikka archive, as opposed to when it is categorized differently
 419 (e.g. here we ignore LPS that are classified as a depression in a reanalysis but a low in the
 420 Sikka archive). These composites are made using ERA5, since that reanalysis was not used
 421 in tuning the tracking algorithm. There are 57 lows and 10 depressions in ERA5 that are
 422 missing from the Sikka archive. Composites are created by averaging, in a storm-centered
 423 reference frame, the three time steps having the largest central MSLP anomaly.

424 The composites of lows and depressions have structures consistent with those seen
 425 in prior studies (Godbole, 1977; Hurley & Boos, 2015), and these exhibit relatively little
 426 differences between matches and non-matches (Figure 4). The LPS all consist of a column
 427 of cyclonic potential vorticity (PV) that extends from the surface to the upper troposphere,
 428 with primary maxima near 500 hPa and secondary peaks around 850 hPa. The composite
 429 relative vorticity is more bottom-heavy, peaking near 800 hPa. Both the PV and relative
 430 vorticity tilt slightly westward with height and are stronger in depressions than in lows,
 431 as expected. For lows, the non-matches (i.e. those present in ERA5 but missing from the
 432 Sikka archive) are weaker than the matches, perhaps because the 850 hPa streamfunction
 433 in ERA5 represents weaker systems than were contained in the MSLP maps on which the
 434 Sikka archive was based, or perhaps because our tracking algorithm was better able to
 435 detect weak systems than the subjective analysis used by the Sikka archive. There is no
 436 clear difference between the composites of matching and non-matching depressions, with any
 437 quantitative differences in magnitude likely not significant considering the low number (10)
 438 of non-matches. Comparisons of composites of winds, relative humidities, and temperatures
 439 yielded similar results (not shown).

440 We furthermore obtained the daily MSLP charts from the IMD, which are thought to
 441 be similar to those on which the Sikka archive was based, and manually inspected these to
 442 search for the ten depressions present in ERA5 but missing in the Sikka archive. At the
 443 times and locations of all ten of these missing depressions, we found LPS-like features in
 444 the pressure charts, with three of the charts clearly showing disturbances marked on the
 445 charts as depressions or a more intense category of LPS. We conclude that the ten additional
 446 depressions in ERA5 are real and were somehow missed when the Sikka archive was created.

447 **4 Assessing the LPS climatology in reanalyses**

448 We now examine the climatological mean distributions of genesis density, track density,
 449 disturbance lifetime, and track length, with the goal of assessing whether the overall statistics
 450 of disturbances identified in reanalyses agree with the well-known statistics of monsoon LPS.

451 **4.1 Genesis**

452 The boreal summer (June-September) distributions of genesis frequency for all LPS
 453 are broadly similar among all reanalyses and the Sikka archive (Figure 5). The latter has
 454 genesis more concentrated over the northern Bay of Bengal, but with a total number of
 455 LPS—14 per summer—similar to that in most of the reanalyses. The total count is higher
 456 in MERRA-2 and CFSR, around 18 per summer.

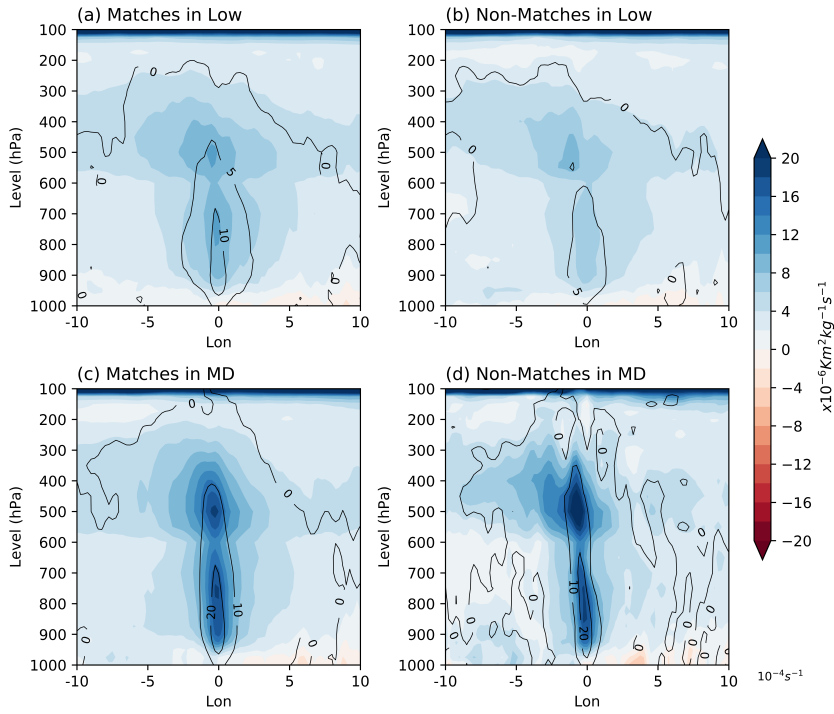


Figure 4. Composite of the vertical cross-section of potential vorticity (shaded) and relative vorticity (contours), through the central longitude of the system, for (a) matches in lows, (b) non-matches in lows, (c) matches in depressions and (d) non-matches in depressions.

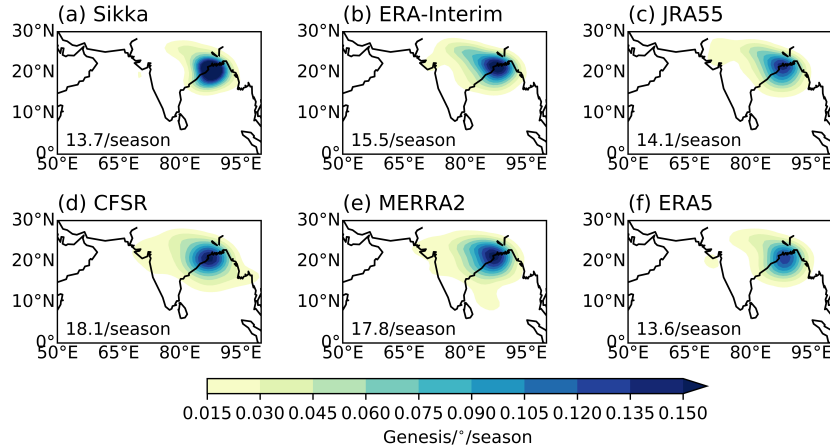


Figure 5. Genesis density of LPS for the period of 1980–2003 in the Sikka archive and reanalyses. Kernel density estimates are used to calculate the genesis density. Numbers in the bottom-left corner represent the mean number of LPS in a season for the period.

There is general agreement amongst the reanalyses, and between the reanalyses and the Sikka archive, regarding the partitioning of LPS into lows and depressions, the rate of genesis over land compared to that over ocean, and the seasonal cycle of genesis (Figure 6). The most notable outlier is MERRA-2 which, unlike the other four reanalyses and the Sikka archive, has more depressions than lows.

462 Consistent with the spatial distributions of genesis shown in Figure 5, most reanalyses
 463 also represent a larger fraction of LPS forming over land, compared to the Sikka archive
 464 (Figure 6). ERA5 has the fewest LPS of all the reanalyses, though the difference is relatively
 465 small, and the ERA5 total count is an almost exact match to the Sikka archive. The match
 466 with the Sikka archive is notable because ERA5 was not included in the algorithm's training
 467 dataset. All the reanalyses also capture the greater frequency of LPS in the middle of
 468 summer, although ERA5 shows slightly greater frequency in July while all other reanalyses
 469 and the Sikka archive show greatest frequency in August. This seems to be an improvement
 470 over previous reanalysis-based tracking algorithms, which showed genesis occurring more
 471 frequently in June than in August in ERA-Interim (Hurley & Boos, 2015).

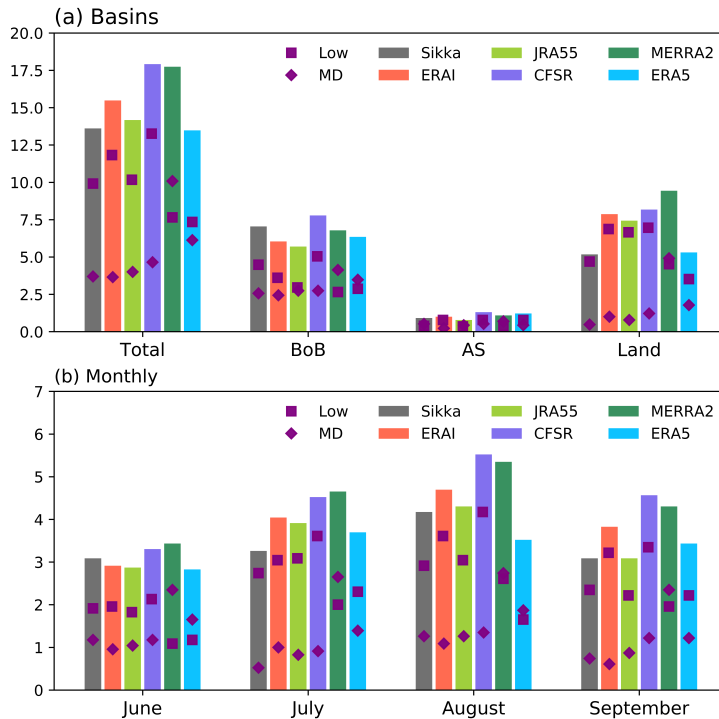


Figure 6. (a) The summer monsoon season (JJAS) climatology, for the Sikka archive and reanalyses, of the number LPS formed over the north Indian Ocean basin and subregions of the Bay of Bengal (BoB), Arabian Sea (AS), and Indian land mass (Land). (b) Climatological monthly variation of LPS. monsoon lows and monsoon depressions are represented as squares and diamonds respectively. The period of analysis is 1980–2003.

4.2 Track density and lifetime of LPS

All the reanalyses show a similar track density distribution to that seen in the Sikka archive, although the reanalyses extend further westward toward northwestern India (Figure 7). The highest track density over land is found in MERRA-2; that reanalysis also has the highest number of days with an LPS present, which is due to both the high genesis frequency and high LPS lifetime in MERRA-2 (Figure 8).

Lifetimes are generally longer in the reanalyses, with the longest found in ERA5, which has LPS lasting one to two days longer than the Sikka archive. The distributions of lifetimes for all LPS are more strongly skewed in the reanalyses than in the Sikka archive, with the median lifetime being almost a full day longer than the mean lifetime (Figure 8a). Track

lengths (in great circle distance between start and end points) are similar between the reanalyses and Sikka archive, implying a slower translation speed in the reanalyses: 2.3 m s^{-1} in the Sikka archive and 1.6 m s^{-1} - 1.91 m s^{-1} in the reanalyses. In all datasets, depressions have longer tracks and lifetimes than lows, and tracks and lifetimes are longer over ocean than over land.

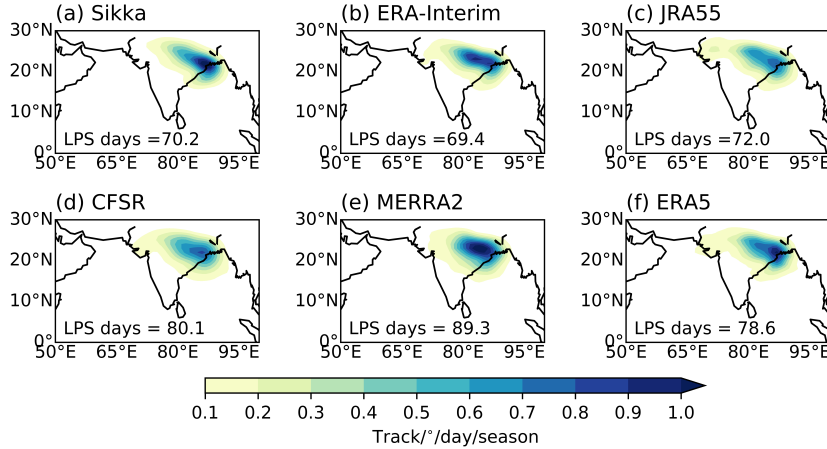


Figure 7. Track density of LPS for the period of 1980-2003 in the Sikka and reanalyses. Kernel density estimates are used to calculate the track density of LPS. Numbers in the bottom-left corner represent the mean number of days in which LPS are present in a season for the period.

5 Interannual and long term variations

5.1 Interannual correlations between datasets

The interannual variability of seasonal total counts of LPS, lows, and depressions has a similar magnitude across reanalyses and the Sikka archive, but these variations exhibit low to modest correlation between data products (Figure 9a-9c). The correlations between different reanalyses of seasonal LPS counts range from about 0.5 to 0.75, higher than the 95% confidence level of 0.34 for this sample size, with the two ECMWF reanalyses being most strongly correlated. Interannual correlations between datasets are weaker for the individual categories of lows and depressions (Figures 9b, c); this is not surprising since differences in the categorization of an LPS as a low vs. a depression can arise from small differences in surface pressure and wind speed. Any negative correlations exist only for these subcategories (e.g. between depression counts in JRA-55 and the Sikka archive (Figure 9c)); and are not statistically significant. The dataset having the weakest correlations with all others is the Sikka archive; the LPS dataset of Hurley and Boos (2015) also showed little interannual correlation with the Sikka archive. This might arise due to differences in the geophysical observations on which each dataset is based, on the variables used for tracking, and on other methodological details. In particular, LPS in the Sikka archive were identified through manual analysis of surface pressure charts, which were in turn obtained through manual analysis of station observations; such subjective methods might introduce random and/or systematic errors (e.g., a bias toward identifying LPS over land).

We now explore the differences that reduce interannual correlations between datasets, using brief statistical modeling to explain how the modest correlations seen in Figure 9 are consistent the seemingly good skill scores shown in Figure 3. We state in Section 3.3 that 67 LPS are present in ERA5 but not in the Sikka archive; these non-matching storms, which account for about 20% of the total number of storms in the record, reduce the interannual

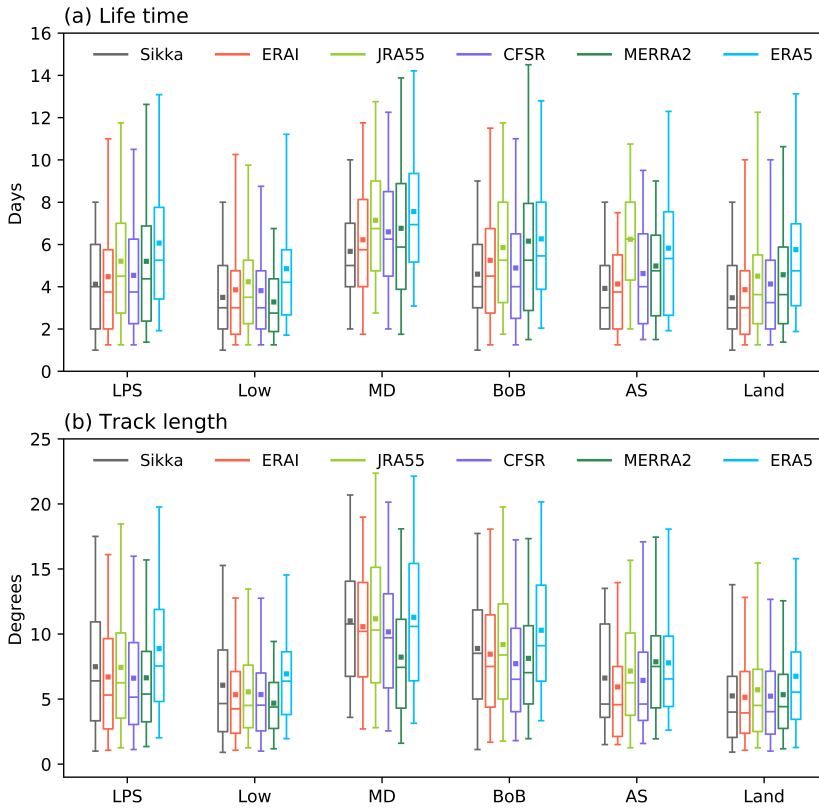


Figure 8. Box-and-whisker plots of (a) lifetime (b) track length of LPS in Sikka archive and all reanalyses. The horizontal line within the boxes indicates the median, boundaries of the boxes indicate the 25th and 75th percentile, the whiskers indicate the 5th and 95th percentile values, and the solid square represents the mean value. The period of analysis is 1980–2003.

correlation between those two datasets. We test the sensitivity of the interannual correlations to missing storms by removing random LPS from the Sikka archive between 1979 and 2003, adding the same number of “false alarm” LPS to random years in that archive, then recalculating the interannual correlation with the original Sikka archive. Removing 67 random storms and adding the same number of false alarms degrades the correlation coefficient from 1.0 to an average of 0.62 (with a 95% confidence interval of 0.36–0.81, empirically sampled from 5,000 iterations). Increasing the fraction of randomly replaced storms to one-third of those in the Sikka archive further degrades the correlation coefficients, in this statistical model, so that the 95% confidence interval is 0.08–0.7, encompassing the correlations between the Sikka archive and most reanalyses. Thus, the relatively low interannual correlation each reanalysis has with our reference dataset is consistent with the hit ratios and false alarm ratios seen in Figure 3. We note that the interannual correlation between the Sikka archive and ERA-Interim (0.53) is higher than reported by Praveen et al. (2015) (0.2 to 0.4); those authors detected LPS using surface pressure, which we show in Section 3.2 produces worse skill than detectors based on streamfunction (which was used in the tracking algorithm examined here).

In summary, the interannual correlation between two datasets can be greatly reduced when a modest fraction of storms in one dataset does not match the other dataset. Our statistical modeling showed that replacing 20–30% of the storms in one dataset with the same number of randomly distributed false alarms can reduce the correlation coefficient to the

532 levels of 0.2-0.5 frequently seen in Figure 9. Thus, even though the reanalyses capture about
 533 80% of LPS in the Sikka archive, we should not expect the interannual correlations between
 534 these datasets to be large. Correlations for the subcategories of lows and depressions will be
 535 further reduced by the fact that one in three depressions in the Sikka archive is categorized
 536 as a low in the reanalyses and vice-versa. Yet there is clearly some agreement: all datasets,
 537 including the Sikka archive, capture the high number of depressions in 2006 (Figure 9d),
 which coincides with an Indian Ocean Dipole event (Krishnan et al., 2011).

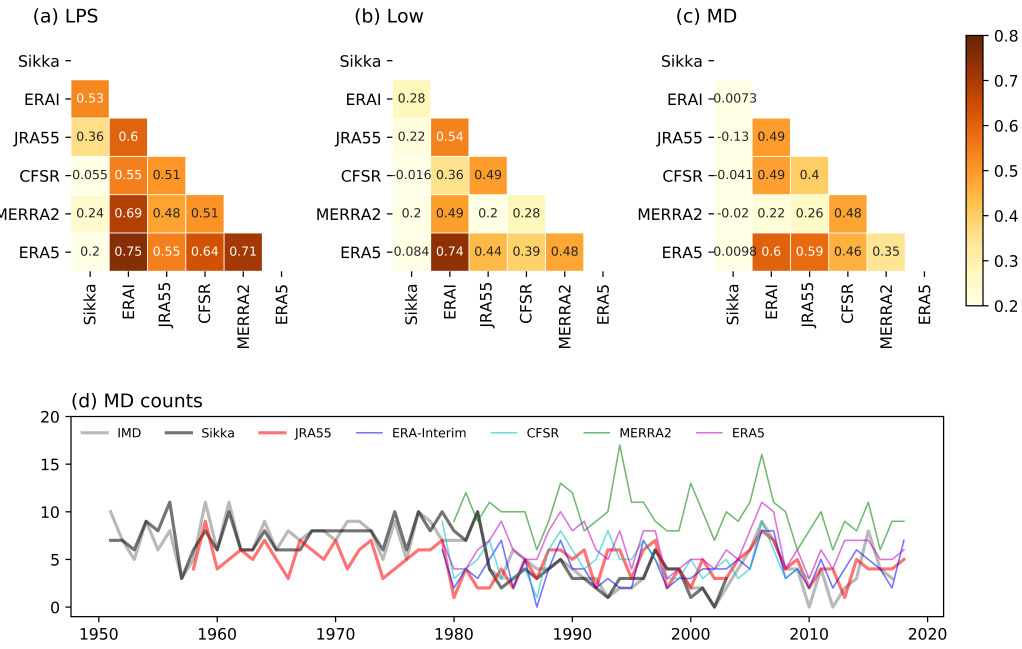


Figure 9. Interannual correlation of the number of Indian summer (June-September) (a) monsoon low-pressure systems (b) lows and (c) monsoon depressions between the datasets includes Sikka archive and the reanalyses during 1980-2003, the years in which all LPS dataset available. (d) Year to year variation in the number of monsoon depression in all renalysis datasets, Sikka archive and from IMD.

538

539

5.2 Relation to interannual climate modes

540 Given the large contribution of LPS to India's total summer rainfall (Yoon & Chen,
 541 2005), some studies have explored whether interannual variations in LPS activity are associated
 542 with interannual variations in total Indian summer rainfall (Sikka, 2006; Krishnamurthy
 543 & Ajayamohan, 2010). We build on this by analyzing how LPS count, mean lifetime, and
 544 track length vary between pluvial and drought years in the Sikka archive and reanalyses.
 545 We define "pluvial" years as years when seasonal total rainfall is more than one standard
 546 deviation above the mean, and "drought" years as those when rainfall is more than one stan-
 547 dard deviation below the mean. LPS counts are significantly higher in pluvial than drought
 548 years in four out of five reanalyses (Figure 10a), but there are no significant changes in
 549 lifetime and track length in four of five reanalyses (Figure S1a and S2a). Although the
 550 Sikka archive shows no change in LPS counts between pluvial and drought years between
 551 1979 and 2003, Krishnamurthy and Ajayamohan (2010) performed the same analysis of the
 552 Sikka archive for 1901-2003 and found a higher number of LPS and a higher number of days
 553 with LPS conditions in pluvial compared to drought years. When examining how counts of

the individual categories of lows and depressions change between pluvial and drought years, most reanalyses and the Sikka archive show no detectable signal (Figure 10b, c). The rainfall produced by depressions is higher in pluvial than in drought years, with the seasonal rainfall accumulation occurring within 8 degrees of an LPS center over Indian land regions differing by 104 ± 96 mm for ERA5 tracks and ERA5 precipitation. For lows and for all LPS, the 95% confidence interval on the difference between pluvial and drought years includes zero (Figure S3). Performing this analysis with other rainfall products and reanalysis datasets is deemed outside the scope of this study.

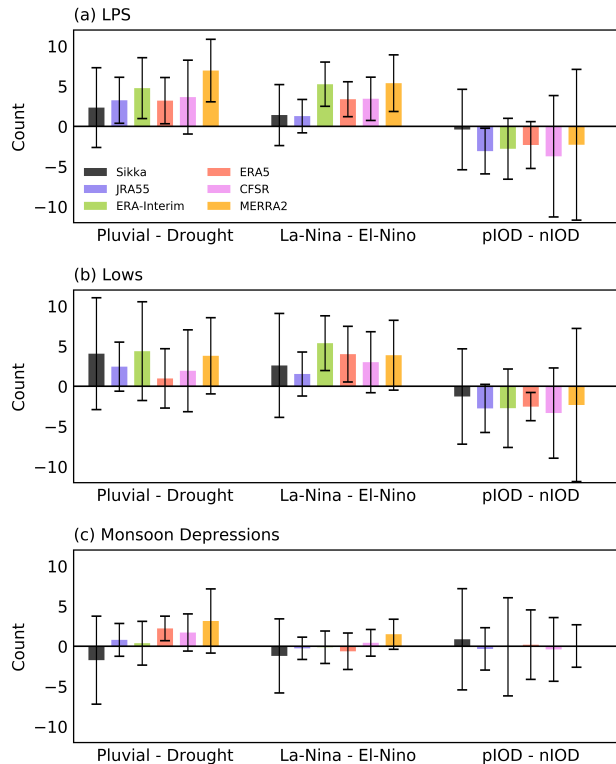


Figure 10. Difference of (a) LPS, (b) lows and (c) monsoon depression mean counts in pluvial-drought summer monsoon years, La Niña-El Niño years, and positive-negative Indian Ocean Dipole years. The vertical lines represent the 95% confidence interval for the difference in the mean counts. Analysis of each dataset set includes all available period of that datsets (see Table 1)

Interannual variation of the Indian summer monsoon is highly linked to ENSO, with an increased propensity for drought years in the warm phase of ENSO (El Niño) and pluvial years in its cold phase (La Niña). We find that LPS counts are higher in La Niña years than El Niño years (Figure 10a), and the differences are significant in all datasets except the Sikka archive and JRA-55. When assessing ENSO-related variations in lifetimes and track lengths, the only detectable signal is in ERA-Interim and ERA5, which exhibit LPS lifetimes that are higher in El Niño years than La Niña years (contrasting with their lower average counts in those years; Figure S1a). The fact that a signal is sometimes detected in only one or two out of six datasets shows that it may be important to reexamine results from prior studies that relied on a single dataset. For example, Krishnamurthy and Ajayamohan (2010) used only the Sikka archive when showing that LPS activity is roughly equal in El Niño and La Niña years. Hunt et al. (2016) relied on only ERA-Interim when finding that depression activity is 16% higher in El Niño than La Niña years.

575 Finally, we examine covariations of LPS with the Indian Ocean Dipole (IOD), an SST
 576 pattern associated with variations in Indian summer monsoon circulation and rainfall (Saji
 577 et al., 1999; Webster et al., 1999). Krishnan et al. (2011) found that depressions have higher
 578 track lengths in positive IOD years, and Hunt et al. (2016) found that depression lifetime
 579 is 12% higher in positive IOD years. We find that only one reanalysis (JRA-55) shows
 580 a change in LPS counts between positive and negative IOD years, and another reanalysis
 581 (CFSR) shows longer depression lifetimes (Figure S1c and S2c). For all other datasets, the
 582 95% confidence interval on the IOD-related changes in counts, lifetimes, and track lengths
 583 includes zero.

584 5.3 Trends in LPS

585 5.3.1 Linear trend analysis

586 Based on the Sikka archive and the IMD dataset of depression counts, previous studies
 587 discussed an apparent increase in the number of lows and a decrease in the number of
 588 depressions forming each summer (Jadhav & Munot, 2009; Prajeesh et al., 2013; Vishnu et
 589 al., 2016, and references therein). However, Cohen and Boos (2014) questioned the existence
 590 of a decrease in the number of depressions in the past 40 years, based on their finding that
 591 no trend in depression counts could be detected in ERA-Interim and on their discovery
 592 of depressions in that reanalysis that were missing in the IMD dataset. Here we examine
 593 whether a trend in the number of LPS overall, or in the number of lows or depressions,
 594 can be detected in any of the track datasets created using our tracking algorithm. We first
 595 assess the period since 1979, since four of our reanalyses start in that year, then compare
 596 to results starting in 1958 (for which only JRA-55, the Sikka archive, and the IMD dataset
 597 provide values).

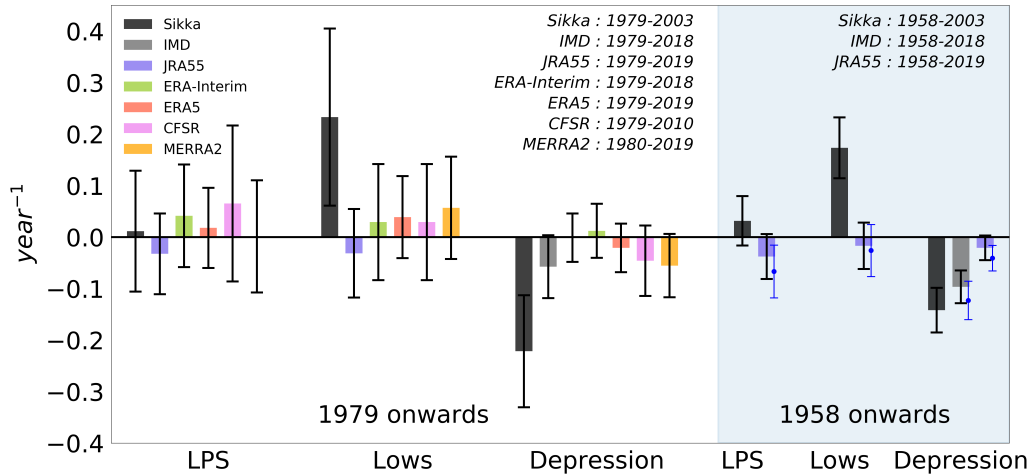


Figure 11. Linear trends in LPS, lows, and depression in the Sikka archive and reanalyses. The white shaded region shows trends from 1979 onwards, while gray shaded region shows trends for 1958 onwards. Error bars represent the 95% confidence interval for these trends. Blue dots and error bars represent the trend and 95% confidence interval, respectively, for the extended season of May to October. The 95% confidence intervals assume a normal distribution and thus are 1.96 times the standard error.

598 Consistent with previous studies, the Sikka archive shows no trend in the seasonal
 599 counts of all LPS since 1979, together with an increasing trend in lows and a decreasing
 600 trend in depressions (Figure 11). Any decreasing trend in depression counts in the IMD

dataset is weaker and has an error bar that includes zero. None of the reanalyses show any appreciable trend in the counts of lows or depressions. Similarly, no significant trend in the total seasonal rainfall produced by LPS, lows, or depression is seen when using ERA5 tracks with ERA5 precipitation (Figure S4); similar trend analyses using other rainfall products will be undertaken in separate work.

Vishnu et al. (2016) noted that the trend in depressions is not linear, but consists mainly of a large reduction around 1980, which lies at the beginning of the records discussed in the previous paragraph. Since JRA-55 is the only reanalysis with data prior to 1979, we compute the trend in depressions for the more extended period starting from 1958 in JRA-55, and compare this with trends from the IMD and Sikka datasets (Figure 11). The IMD and Sikka datasets show depression counts decreasing at a rate of -0.096 year^{-1} and -0.14 year^{-1} , respectively (with 95% confidence intervals of $\pm 0.032 \text{ year}^{-1}$ and $\pm 0.043 \text{ year}^{-1}$; Figure 11, and see the time series in Figure 9d). The long-term decrease in depressions in the Sikka archive is opposed by a long-term increase in lows, resulting in no trend in total LPS. Any trend in JRA-55 is substantially smaller than in the Sikka or IMD datasets and is not significant at the 95% confidence level (Figure 11); the trend in count of depression in JRA-55 is -0.021 year^{-1} with a 95% confidence interval of $\pm 0.024 \text{ year}^{-1}$). No statistically significant trend is seen in the total number of LPS forming each summer in JRA-55.

Although the Indian summer monsoon season is commonly defined as occurring June-September, with the Sikka archive available for only those months, it is possible that the results of our trend analysis would change if we used an extended season of May-October. Indeed, Xavier et al. (2007) argued that the primary effect of ENSO on Indian rainfall occurs via its influence on the duration of the rainy season, with La Niña events allowing it to extend into May and October. Including May and October in our trend analysis for the period starting in 1958 yields an increase in the magnitude of the depression count trends found in JRA-55 and the IMD dataset, with the JRA-55 trend becoming significant at the 95% confidence level (Figure 11). The total number of LPS forming in this extended summer season in JRA-55 also shows a decreasing trend that is significant at the 95% confidence level, but there is no discernible trend in lows in JRA-55. We also repeated the trend assessment, using the longer May-October season, for all reanalyses for the shorter period starting in 1979, with little change in the results: only ERA-Interim LPS show an increasing trend significant at the 95% confidence level.

We also analyze storm count trends using multiple detection algorithms, in order to explore the influence of parametric and structural uncertainty in the algorithm on our trend assessment. Specifically, we examine LPS counts obtained using the top five streamfunction-based algorithms, the top three geopotential height-based algorithms, and the top three MSLP-based algorithms. No algorithms applied to any reanalysis show a significant trend starting in 1979 (Figure S5). However, two of the nine algorithms applied to JRA-55 show a statistically significant decrease in LPS from 1958, and one of the nine shows a significant decrease in depression counts in that period. All of these trends are of similar magnitude to those found in JRA-55 with our primary algorithm (Figure 11).

5.3.2 Change point detection

Like any reanalysis, JRA-55 assimilated data from an observational network that evolved over time, and we wish to consider whether this might affect any detected trends. For example, satellite data first started to be assimilated by JRA-55 around 1980, and there is a large reduction in depression counts in JRA-55 in that year (Figure 9d). We calculate the year and magnitude of a single long-term shift in the summer mean depression count using a binary change point detection method (Truong et al., 2019), and find that the mean depression count undergoes a systematic reduction in the early 1980s all datasets: 1983 in IMD and the Sikka archive and 1980 in JRA-55 (Figure 12). The shift in the mean values is larger in the IMD dataset (decreasing from $7.5 \pm 0.7 \text{ year}^{-1}$ to $3.6 \pm 0.7 \text{ year}^{-1}$) and the

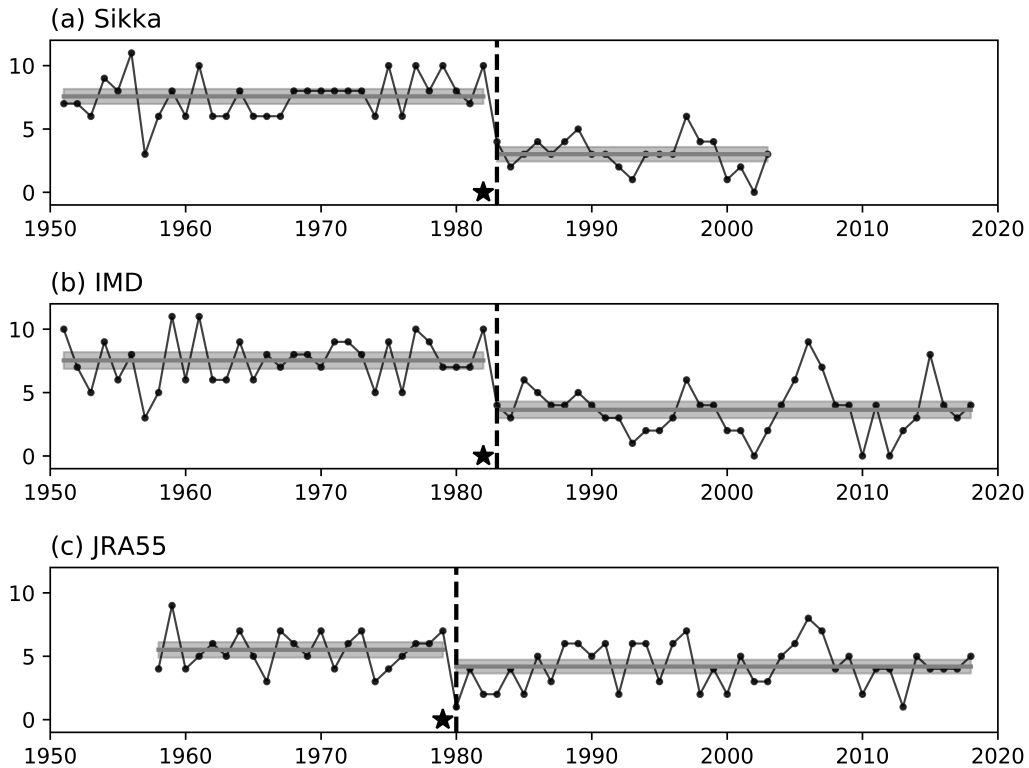


Figure 12. Illustration of a shift in depression count around 1980. Year-to-year variation of depression count (black line) in (a) Sikka archive, (b) IMD and (c) JRA-55. The vertical dash line is the year of mean shift in the depression count using binary change point detection. The star symbol represents the introduction of the geostationary satellites in the respective dataset. The horizontal grey line shows the annual mean value of depression count in the given epoch, and shading shows the 95% confidence interval of the mean value.

Sikka archive (decreasing from $7.6 \pm 0.6 \text{ year}^{-1}$ to $3.0 \pm 0.6 \text{ year}^{-1}$) and smallest in JRA-55 (decreasing from $5.5 \pm 0.6 \text{ year}^{-1}$ to $4.2 \pm 0.5 \text{ year}^{-1}$). The shifts in all three data sets are statistically significant at the 95% confidence level. The shift in JRA-55 in 1980 is contemporaneous with the introduction of geostationary satellite observations to that reanalysis system in 1979 (Ebita et al., 2011), the date marked by the star in Figure 12c. Similarly, the IMD started using Indian geostationary satellite data in 1982, which is contemporaneous with the 1983 shift in depression counts in both the Sikka archive and the IMD dataset (recall that the Sikka archive was constructed by analyzing MSLP maps obtained from the IMD). This suggests that the shift, and by association the linear trends discussed above, might be an artifact of changes in observational data sources. Formal attribution of these early-1980's shifts is beyond the scope of this manuscript, but these results suggest that further study is warranted.

6 Summary and conclusions

Synoptic-scale monsoon LPS produce abundant rainfall over South Asia, making the identification of LPS in estimates of past and future atmospheric states an important task. Yet previous methods for tracking LPS have relied on subjective or automated methods not systematically assessed for skill or optimality (Mooley & Shukla, 1987; Sikka, 2006; Praveen

et al., 2015; Hurley & Boos, 2015; Hunt et al., 2016). For example, multiple previous LPS datasets were based entirely on MSLP, even though LPS are known to have peak intensities several kilometers above the surface (Godbole, 1977). These issues become especially salient when examining multi-decadal trends in LPS activity, because unintentional changes in a subjective method or trends in the observing network on which an underlying dataset is based could bias an analyzed trend.

This study builds on previous literature by introducing a fast and objective tracking algorithm able to identify monsoon LPS in high-resolution datasets. The method is based on the feature tracking capabilities of the TempestExtremes package. A sensitivity analysis was performed to choose an optimal algorithm using multiple reanalyses of various spatial and temporal resolutions. A total of 512 algorithms (defined by different search variables and values for the closed contour criteria) are applied to four reanalyses for the training period of 1990-2003. Based on a skill score, the CSI, that compares the reanalyses with each other and with the Sikka archive (our reference dataset), the optimal algorithm was found to use the 850 hPa streamfunction. The LPS identified with this algorithm in reanalyses are found to about than 80% of LPS in the Sikka archive. The reanalyses track datasets also contain LPS not present in the Sikka archive. For instance, the ERA5 dataset includes 57 lows and 10 depressions that are entirely missing in the Sikka archive. Composites of these LPS and the LPS present in the Sikka archive show similar dynamical structures, so we conclude that the algorithm correctly captures LPS in the atmospheric states represented by the reanalyses.

Characteristics of the LPS, including distributions of genesis frequency, track density, intensity, lifetime, and track length, are consistent across all reanalyses and are similar to results from the Sikka archive. The new reanalysis track datasets also reproduce previously reported monthly and basin-wise climatological variations of LPS characteristics. On interannual time scales, LPS counts in the reanalyses have weak correlation with the Sikka archive. This result may be due, in part, to LPS that are missing from the Sikka archive but that exist in most of the reanalyses. Indeed, we estimate that if only 20-30% of the storms in one dataset are replaced with randomly distributed false alarms, this is expected to reduce the interannual correlation coefficient to 0.5 or lower. The better correspondence between the track datasets based on five different reanalyses, with horizontal resolutions ranging from 0.25° to 1.25° , gives confidence that the algorithm can consistently capture LPS in datasets with different resolutions.

Our examination of interannual variations in LPS genesis frequency, track length, and lifetimes illustrate the importance of assessing signals in multiple datasets. For the period starting in 1979, we find significantly higher LPS counts in pluvial years compared to drought years in four out of five reanalyses, in agreement with the longer period (1901-2003) analysis of Krishnamurthy and Ajayamohan (2010). We also find significantly higher LPS counts in La Niña years relative to El Niño years, again in four of five reanalyses and consistent with Krishnamurthy and Ajayamohan (2010). Associations between LPS counts and the Indian Ocean Dipole are detected in only one reanalysis, despite the fact that Krishnan et al. (2011) and Hunt et al. (2016) reported enhanced depression activity in positive IOD years. The higher depression activity in El Niño years reported by Hunt et al. (2016) was also not seen in any of the reanalyses we examined.

Past studies of long-term trends in the IMD and Sikka datasets have found increases in the number of lows and decreases in the number of depressions (Rajendra Kumar & Dash, 2001; Prajeesh et al., 2013; Vishnu et al., 2016). Here, however, we do not detect statistically significant trends in summer counts of lows or depressions in any reanalysis for the period from 1979 onwards (the Sikka archive has a strong decrease in depression counts and an increase in lows for that period). The JRA-55 reanalysis, which provides data starting in 1958, shows a statistically significant reduction in depression counts only when using an extended summer season (May-October), and this trend is about one-quarter the magnitude of the trend seen in the IMD dataset and Sikka archive. Furthermore, a binary

722 change point detection analysis shows that the long-term decrease is consistent with a step-
 723 wise reduction in depression counts in the year following the introduction of geostationary
 724 satellite data into the datasets underlying the IMD, Sikka, and JRA-55 products. This
 725 suggests the possibility that no long-term reduction in depressions has occurred, and trends
 726 seen in existing data products may be artifacts of change in the observing network; further
 727 analysis is warranted.

728 The new and objective LPS datasets developed here have been made publicly available,
 729 together with the tracking algorithm, to allow their broad use in characterizing LPS activ-
 730 ity and understanding LPS dynamics ([doi:10.5281/zenodo.3890646](https://doi.org/10.5281/zenodo.3890646)). These datasets and
 731 the tracking algorithm may also be useful in assessing LPS activity in ensembles of global
 732 climate models and in characterizing and correcting bias in forecasts made by numerical
 733 weather prediction models. The future release of new reanalysis data for years preceding
 734 1979, such as is expected for ERA5 (Hersbach & Dee, 2016), will also provide new oppor-
 735 tunities to reexamine long-term trends in LPS activity, especially since those reanalyses
 736 include representations of historical climate forcings by greenhouse gas, aerosol, and land
 737 use changes.

738 Appendix A Boundary conditions for streamfunction inversion

739 A practical challenge exists when computing the streamfunction, ψ , of the horizontal
 740 wind, \vec{u} on a level of a vertical coordinate system that intersects the ground: boundary
 741 conditions must be imposed on that intersection when inverting the winds (or vorticity) to
 742 obtain ψ . That is, the uniqueness of the Helmholtz decomposition that holds in a spherical
 743 domain without boundaries breaks down, and a class of harmonic functions can be added to
 744 ψ while still allowing $\nabla^2\psi$ to correctly represent the local vertical vorticity. Numerous ways
 745 of dealing with this nonuniqueness have been proposed in the context of atmospheric and
 746 oceanic flow (Lynch, 1988). One method requires the velocity potential, ϕ to vanish on the
 747 boundaries, minimizing the kinetic energy in the divergent part of the flow (Sangster, 1960;
 748 Pedersen, 1971). Another method requires ψ to be constant along a boundary (Watterson,
 749 2001); this is appropriate when there is zero horizontal divergence along the boundary but
 750 is invalid in many cases having large vertical motion along physical boundaries, such as
 751 up-welling in coastal ocean regions (Li et al., 2006) or strong orographic ascent in the
 752 atmosphere. Lynch (1989) proposed a three-component partitioning into nondivergent, ir-
 753 rotational, and harmonic flow, while Li et al. (2006) made the two-component decomposition
 754 unique by introducing a constraint to the inversion problem that implicitly determines the
 755 boundary condition by minimizing the joint amplitude of ψ and ϕ .

756 Here we are concerned with domain boundaries created by the intersection of a pres-
 757 sure surface with topography, with the pressure surface lying at a sufficiently high altitude
 758 that the boundaries surround relatively small holes in the otherwise global, spherical do-
 759 main. Unlike the regional atmospheric model problem in which ψ and ϕ are obtained in a
 760 subdomain of global, nonzero atmospheric flow, we know that no wind exists outside of our
 761 domain (i.e. beneath Earth's surface). We thus follow the suggestion of Morse and Feshbach
 762 (1953) and set the total wind outside the domain boundaries to zero and invert \vec{u} to obtain
 763 unique distributions of ψ and ϕ in the unbounded global domain. Some reanalyses (e.g.
 764 ERA-Interim) extrapolate winds beneath Earth's surface, so our choice involves replacing
 765 those extrapolated values with $\vec{u} = 0$. This choice results in nonzero values of the nondiver-
 766 gent and irrotational wind beneath Earth's surface; these two components sum to zero in
 767 that region. This contrasts with methods that assumed nondivergent flow along the bound-
 768 aries (Watterson, 2001), because we recognize that winds can horizontally converge along
 769 the topographic boundary at the grid scale of the data; such convergence is common along
 770 the Himalaya and Arakan mountains in the summer monsoon. An important point is that
 771 our choice of \vec{u} beneath Earth's surface, or equivalently of the boundary condition for ψ , has
 772 only minor effects on our numerical identification of vortices because that choice alters ψ

773 only by addition of a function with zero curvature, and our identification algorithm involves
 774 finding local minima (i.e. regions of positive curvature) in the discretized streamfunction.

775 Appendix B LPS detection program

776 The command line syntax to obtain LPS tracks from a six-hourly dataset using Tem-
 777 pestExtremes with a bash shell is:

```

778 # Set a series of shell variables:
779 # File containing Streamfunction at 850 (PSI)
780 psifile="./psi.nc"
781
782 # File containing mean sea level pressure (msl)
783 pslfile="./msl.nc"
784
785 # File containing relative humidity at 850 hPa (RH)
786 rhfile="./RH850.nc"
787
788 # File containing surface wind field (u10, v10)
789 uvfile="./uvsurf.nc"
790
791 # File containing surface geopotential (zs)
792 zsfile="./geopotential_surface.nc"
793
794 # File containing land-sea fraction (lsm)
795 lsmfile="./land_sea.nc"
796
797 # Candidate file
798 candidatefile="./LPS_candidates.txt"
799
800 # Output file
801 outfile="./LPS_output.txt"
802
803 # Track file
804 trackfile="./LPS_track.txt"
805
806 # Detect LPS:
807 #   1) Search for candidates as minima in the streamfunction field
808 #   2) Merge candidates within 5 degrees
809 #   3) Output streamfunction minima at the candidate point,
810 #      sea level pressure minima within 3 degrees of the candidate point,
811 #      wind speed maxima within 3 degrees of candidate,
812 #      relative humidity averaged over the area within 3 degrees of candidate,
813 #      surface geopotential maximum within 2 degrees of candidate,
814 #      land-sea ratio at candidate point, and
815 #      minimum sea level pressure location.
816 $path-to-TEMPEST-bin/DetectNodes
817   --in_data "$psifile;$pslfile;$rhfile;$uvfile;$zsfile;$lsmfile"
818   --out $candidatefile
819   --searchbymin "PSI" --mergedist 5.0
820   --closedcontourcmd "PSI,12.5e5,10,0"
821   --outputcmd "PSI,min,0;msl,min,3;RH,avg,3;zs,max,2;lsm,max,0;
822     _VECMAG(u10,v10),max,3;msl,minix,3.0"
```

```

824 #Stitch candidates to make tracks:
825 # 1) With a maximum distance of 3.0 degrees between in-sequence candidates
826 # 2) With a minimum length of 5 time points
827 #     (ensures track lasts longer than 1 day in six-hourly data)
828 # 3) With a maximum gap size of 2 time points (12 hours)
829 # 4) With the surface geopotential maximum less than 8000 m^2 s^{-2}
830 #     for at least 4 time steps along the track
831 # 5) With the relative humidity higher than 85% for at least 4 time steps
832 #     along the track.
833
834 $path-to-TEMPEST-bin/StitchNodes --in $candidatefile --out $outfile
835     --format "i,j,lon,lat,strf850,slp,rh,zs,lsm,sp,minmslix"
836     --range 3.0 --minlength 5 --maxgap 2
837     --threshold "zs,<=,8000.,4;rh,>=,85,4"
838
839 # Calculate some derived quantities using track data:
840 # count the closed contours of MSLP, calculate ACEPSL, ACE, PDI, IKE
841 # ACEPSL = 1e-4 * (1.94384 kt/(m/s) * (3.92 * (1016 - PSL)^0.644))^2
842 # if PSL < 1016. Here PSL is the minimum surface pressure at the point
843 # of detection in hPa. This formula leverages the TC wind-pressure
844 # relationship to provide a proxy for ACE.
845 # ACE = 1e-4 * (1.94384 kt/(m/s) * Umax)^2, where Umax is the maximum
846 # instantaneous wind speed magnitude within the three degree radius (in m/s).
847 # PDI = Umax^3, where Umax is the maximum instantaneous windspeed magnitude
848 # within the three degree radius (in m/s)
849 # IKE = sum_i 0.5 * U_i^2 * area_i, where the sum is taken over all grid boxes
850 # within the given radius, U_i is the wind magnitude in that grid cell,
851 # and area_i is the area of the grid cell (in m^2).
852
853 $path-to-TEMPEST-bin/NodeFileEditor --in_file $outfile --out_file $trackfile
854     --in_data "$pslfile;$uvfile"
855     --in_fmt "lon,lat,strf850,slp,rh,zs,lsm,sp,minmslix"
856     --calculate "deltaslp=max_closed_contour_delta(msl,10,minmslix);
857         acepsl=eval_acepsl(msl,10.0);
858         ace=eval_ace(u10,v10,3.0);
859         pdi=eval_pdi(u10,v10,3.0);
860         ike=eval_ike(u10,v10,3.0)"
861     --out_fmt "lon,lat,strf850,slp,deltaslp,sp,rh,zs,lsm,acepsl,ace,pdi,ike"

```

861 Acknowledgments

862 The authors gratefully acknowledge the financial support given by the Earth System Science Organization, Ministry of Earth Sciences, Government of India (Grant no. IITM/MM-II/Univ_California_USA/INT-3) to conduct this research under Monsoon Mission. This material is based upon work supported by the U.S. Department of Energy, Office of Science, Office of Biological and Environmental Research, Climate and Environmental Sciences Division, Regional & Global Model Analysis Program, under Award Number DE-AC02-05CH11231. It used resources of the National Energy Research Scientific Computing Center (NERSC), which is a DOE Office of Science User Facility.

870 The India Meteorological Department record of monsoon depression tracks was downloaded from the IMD website at <http://www.imd.gov.in>. The Sikka archive was obtained from Sikka (2006). The ERA-Interim dataset was downloaded from the ECMWF website at <https://apps.ecmwf.int/datasets/data/interim-full-daily>. The MERRA-2 dataset was downloaded from NASA's Goddard Earth Sciences Data and Information Ser-

875 vices Center (GES DISC) website at <https://disc.gsfc.nasa.gov/datasets?keywords=%22MERRA-2%22&page=1&source=Models%2FAnalyses%20MERRA-2>. The ERA5 dataset
 876 was obtained from the Copernicus Climate Change Service Climate Data Store (CDS)
 877 website at <https://cds.climate.copernicus.eu/cdsapp#!/home>, accessed on 01-Mar-
 878 2019. The CFSR and JRA-55 reanalysis were obtained from the Research Data Archive
 879 that is maintained by the Computational and Information Systems Laboratory at the
 880 National Center for Atmospheric Research (NCAR). The data are available at <http://rda.ucar.edu>. The HadISST dataset was downloaded from the website of NCAR at
 881 <https://climatedataguide.ucar.edu/climate-data/sst-data-hadisst-v11>.
 882
 883

884 The track datasets created in this work are available through the Zenodo repository,
 885 doi:10.5281/zenodo.3890646

886 References

- Bengtsson, L., Böttger, H., & Kanamitsu, M. (1982). Simulation of hurricane-type vortices
 887 in a general circulation model. *Tellus*, 34(5), 440–457.
- Berry, G. J., Reeder, M. J., & Jakob, C. (2012). Coherent synoptic disturbances in the
 888 Australian monsoon. *Journal of Climate*, 25(24), 8409–8421.
- Bollasina, M., & Nigam, S. (2009). Indian Ocean SST, evaporation, and precipitation
 889 during the South Asian summer monsoon in IPCC-AR4 coupled simulations. *Climate
 890 Dynamics*, 33(7-8), 1017.
- Boos, W., Hurley, J., & Murthy, V. (2015). Adiabatic westward drift of Indian monsoon
 891 depressions. *Quarterly Journal of the Royal Meteorological Society*, 141(689), 1035–
 892 1048.
- Broccoli, A., & Manabe, S. (1990). Can existing climate models be used to study anthro-
 893 pogenic changes in tropical cyclone climate? *Geophysical Research Letters*, 17(11),
 894 1917–1920.
- Chavas, D. R., Reed, K. A., & Knaff, J. A. (2017). Physical understanding of the tropical
 895 cyclone wind-pressure relationship. *Nature Communications*, 8(1), 1–11.
- Cohen, N. Y., & Boos, W. R. (2014). Has the number of Indian summer monsoon depressions
 896 decreased over the last 30 years? *Geophysical Research Letters*, 41(22), 7846–7853.
- Dee, D. P., Uppala, S., Simmons, A., Berrisford, P., Poli, P., Kobayashi, S., ... others
 897 (2011). The ERA-Interim reanalysis: Configuration and performance of the data
 898 assimilation system. *Quarterly Journal of the Royal Meteorological Society*, 137(656),
 899 553–597.
- Delgado, S., Landsea, C. W., & Willoughby, H. (2018). Reanalysis of the 1954–63 Atlantic
 900 hurricane seasons. *Journal of Climate*, 31(11), 4177–4192.
- Di Luca, A., Evans, J. P., Pepler, A., Alexander, L., & Argüeso, D. (2015). Resolution
 901 sensitivity of cyclone climatology over eastern Australia using six reanalysis products.
 902 *Journal of Climate*, 28(24), 9530–9549.
- Ebita, A., Kobayashi, S., Ota, Y., Moriya, M., Kumabe, R., Onogi, K., ... others (2011).
 903 The Japanese 55-year reanalysis “JRA-55”: an interim report. *Sola*, 7, 149–152.
- Gelaro, R., McCarty, W., Suárez, M. J., Todling, R., Molod, A., Takacs, L., ... others
 904 (2017). The Modern-Era Retrospective Analysis for Research and Applications, Ver-
 905 sion 2 (MERRA-2). *Journal of Climate*, 30(14), 5419–5454.
- Godbole, R. V. (1977). The composite structure of the monsoon depression. *Tellus*, 29(1),
 906 25–40.
- Hagen, A. B., Strahan-Sakoskie, D., & Luckett, C. (2012). A Reanalysis of the 1944–53
 907 Atlantic Hurricane Seasons—The first Decade of Aircraft Reconnaissance. *Journal of
 908 Climate*, 25(13), 4441–4460.
- Hersbach, H., Bell, W., Berrisford, P., Horányi, A., J., M.-S., Nicolas, J., ... Dee, D.
 909 (2019). Global reanalysis: goodbye ERA-Interim, hello ERA5. , 17-24. Retrieved
 910 from <https://www.ecmwf.int/node/19027> doi: 10.21957/vf291hehd7

- Hersbach, H., & Dee, D. (2016). ERA5 reanalysis is in production, ECMWF Newsletter 147, ECMWF. *Reading, UK.*
- Hodges, K. I. (1995). Feature tracking on the unit sphere. *Monthly Weather Review*, 123(12), 3458–3465.
- Hodges, K. I. (1998). Feature-point detection using distance transforms: Application to tracking tropical convective complexes. *Monthly Weather Review*, 126(3), 785–795.
- Houze Jr, R., Rasmussen, K., Medina, S., Brodzik, S., & Romatschke, U. (2011). Anomalous atmospheric events leading to the summer 2010 floods in Pakistan. *Bulletin of the American Meteorological Society*, 92(3), 291–298.
- Hunt, K. M., Turner, A. G., Inness, P. M., Parker, D. E., & Levine, R. C. (2016). On the structure and dynamics of Indian monsoon depressions. *Monthly Weather Review*, 144(9), 3391–3416.
- Hurley, J. V., & Boos, W. R. (2015). A global climatology of monsoon low-pressure systems. *Quarterly Journal of the Royal Meteorological Society*, 141(689), 1049–1064.
- India Meteorological Department. (2011). *Tracks of cyclones and depressions over North Indian Ocean (from 1891 onwards)*, Tech. Note Version 2.0. Cyclone Warning and Research Centre India Meteorological Department Regional Meteorological Centre, Chennai, India.
- Jadhav, S., & Munot, A. (2009). Warming SST of Bay of Bengal and decrease in formation of cyclonic disturbances over the Indian region during southwest monsoon season. *Theoretical and Applied Climatology*, 96(3-4), 327–336.
- Kobayashi, S., Ota, Y., Harada, Y., Ebita, A., Moriya, M., Onoda, H., ... others (2015). The JRA-55 reanalysis: General specifications and basic characteristics. *Journal of the Meteorological Society of Japan. Ser. II*, 93(1), 5–48.
- Krishnamurthy, V., & Ajayamohan, R. (2010). Composite structure of monsoon low pressure systems and its relation to Indian rainfall. *Journal of Climate*, 23(16), 4285–4305.
- Krishnan, R., Ayantika, D., Kumar, V., & Pokhrel, S. (2011). The long-lived monsoon depressions of 2006 and their linkage with the Indian Ocean Dipole. *International Journal of Climatology*, 31(9), 1334–1352.
- Landsea, C. W., Glenn, D. A., Bredemeyer, W., Chenoweth, M., Ellis, R., Gamache, J., ... others (2008). A reanalysis of the 1911–20 Atlantic hurricane database. *Journal of Climate*, 21(10), 2138–2168.
- Landsea, C. W., Hagen, A., Bredemeyer, W., Carrasco, C., Glenn, D. A., Santiago, A., ... Dickinson, M. (2014). A reanalysis of the 1931–43 Atlantic hurricane database. *Journal of climate*, 27(16), 6093–6118.
- Li, H., Chen, W., & Shen, I.-F. (2006). Segmentation of discrete vector fields. *IEEE Transactions on Visualization and Computer Graphics*, 12(3), 289–300.
- Lynch, P. (1988). Deducing the wind from vorticity and divergence. *Monthly Weather Review*, 116(1), 86–93.
- Lynch, P. (1989). Partitioning the wind in a limited domain. *Monthly Weather Review*, 117(7), 1492–1500.
- Manganello, J. V., Cash, B. A., Hodges, K. I., & Kinter, J. L. (2019). Seasonal forecasts of North Atlantic tropical cyclone activity in the North American multi-model ensemble. *Climate Dynamics*, 53(12), 7169–7184.
- McCarty, W., Coy, L., Gelaro, R., Huang, A., Merkova, D., Smith, E., ... Wargan, K. (2016). MERRA-2 input observations: Summary and assessment. *NASA Tech. Rep. Series on Global Modeling and Data Assimilation*, NASA/TM-2016-104606, 46, 64.
- Michaelis, A. C., & Lackmann, G. M. (2019). Climatological Changes in the Extratropical Transition of Tropical Cyclones in High-Resolution Global Simulations. *Journal of Climate*, 32(24), 8733–8753.
- Mooley, D. A. (1973). Some aspects of Indian monsoon depression and associated rainfall. *Monthly Weather Review*, 101, 271–280.
- Mooley, D. A., & Shukla, J. (1987). *Characteristics of the westward-moving summer monsoon low pressure systems over the Indian region and their relationship with the monsoon rainfall*. University of Maryland, Department of Meteorology, Center for Ocean-

- 981 Land
- 982 Morse, P., & Feshbach, H. (1953). *Methods of Theoretical Physics* [Vol 1-2].
- 983 Pedersen, K. (1971). Balanced systems of equations for the atmospheric motion- A numerical
984 experiment, and an analytical discussion(Linearized two level model for atmospheric
985 motion equations systems, using Psi-balanced system for 24 hour forecast). *Geofysiske
986 Publikasjoner(Geophysica Norvegica)*, 28, 1–12.
- 987 Prajeesh, A., Ashok, K., & Rao, D. B. (2013). Falling monsoon depression frequency: A
988 Gray-Sikka conditions perspective. *Scientific Reports*, 3, 2989.
- 989 Praveen, V., Sandeep, S., & Ajayamohan, R. (2015). On the relationship between mean
990 monsoon precipitation and low pressure systems in climate model simulations. *Journal
991 of Climate*, 28(13), 5305–5324.
- 992 Rácz, Z., & Smith, R. K. (1999). The dynamics of heat lows. *Quarterly Journal of the
993 Royal Meteorological Society*, 125(553), 225–252.
- 994 Rajendra Kumar, J., & Dash, S. (2001). Interdecadal variations of characteristics of monsoon
995 disturbances and their epochal relationships with rainfall and other tropical features.
996 *International Journal of Climatology*, 21(6), 759–771.
- 997 Ramage, C. S. (1971). *Monsoon meteorology (international geophysics series; v. 15)*. Aca-
998 demic Press.
- 999 Ramanathan, V., Chung, C., Kim, D., Bettge, T., Buja, L., Kiehl, J., ... Wild, M. (2005).
1000 Atmospheric brown clouds: Impacts on South Asian climate and hydrological cycle.
1001 *Proceedings of the National Academy of Sciences*, 102(15), 5326–5333.
- 1002 Rastogi, D., Ashfaq, M., Leung, L. R., Ghosh, S., Saha, A., Hodges, K., & Evans, K. (2018).
1003 Characteristics of Bay of Bengal monsoon depressions in the 21st century. *Geophysical
1004 Research Letters*, 45(13), 6637–6645.
- 1005 Rayner, N., Parker, D. E., Horton, E., Folland, C. K., Alexander, L. V., Rowell, D., ...
1006 Kaplan, A. (2003). Global analyses of sea surface temperature, sea ice, and night
1007 marine air temperature since the late nineteenth century. *Journal of Geophysical
1008 Research: Atmospheres*, 108(D14).
- 1009 Saha, S., Moorthi, S., Pan, H.-L., Wu, X., Wang, J., Nadiga, S., ... others (2010). The
1010 NCEP climate forecast system reanalysis. *Bulletin of the American Meteorological
1011 Society*, 91(8), 1015–1058.
- 1012 Saji, N., Goswami, B., Vinayachandran, P., & Yamagata, T. (1999). A dipole mode in the
1013 tropical Indian Ocean. *Nature*, 401(6751), 360.
- 1014 Sandeep, S., Ajayamohan, R., Boos, W. R., Sabin, T., & Praveen, V. (2018). Decline and
1015 poleward shift in Indian summer monsoon synoptic activity in a warming climate.
1016 *Proceedings of the National Academy of Sciences*, 115(11), 2681–2686.
- 1017 Sanders, F. (1984). Quasi-geostrophic diagnosis of the monsoon depression of 5–8 July 1979.
1018 *Journal of the Atmospheric Sciences*, 41(4), 538–552.
- 1019 Sangster, W. E. (1960). A method of representing the horizontal pressure force without
1020 reduction of station pressures to sea level. *Journal of Meteorology*, 17(2), 166–176.
- 1021 Sikka, D. (1978). Some aspects of the life history, structure and movement of monsoon
1022 depressions. In *Monsoon dynamics* (pp. 1501–1529). Springer.
- 1023 Sikka, D. (2006). *A study on the monsoon low pressure systems over the Indian region
1024 and their relationship with drought and excess monsoon seasonal rainfall*. Center for
1025 Ocean-Land-Atmosphere Studies, Center for the Application of Research on the En-
1026 vironment.
- 1027 Thorncroft, C., & Hodges, K. (2001). African easterly wave variability and its relationship
1028 to Atlantic tropical cyclone activity. *Journal of Climate*, 14(6), 1166–1179.
- 1029 Truong, C., Oudre, L., & Vayatis, N. (2019). Selective review of offline change point
1030 detection methods. *Signal Processing*, 107299.
- 1031 Ullrich, P. A., & Zarzycki, C. M. (2017). TempestExtremes: A framework for scale-
1032 insensitive pointwise feature tracking on unstructured grids. *Geoscientific Model De-
1033 velopment*, 10(3), 1069.
- 1034 Vishnu, S., Francis, P., Shenoi, S., & Ramakrishna, S. (2016). On the decreasing trend of
1035 the number of monsoon depressions in the Bay of Bengal. *Environmental Research*

- 1036 Letters, 11(1), 014011.
- 1037 Vishnu, S., Francis, P. A., Shenoi, S. C., & Ramakrishna, S. S. V. S. (2018). On the
1038 relationship between the Pacific Decadal Oscillation and monsoon depressions over
1039 the Bay of Bengal. *Atmospheric Science Letters*, 19(7), e825.
- 1040 Watterson, I. (2001). Decomposition of global ocean currents using a simple iterative
1041 method. *Journal of Atmospheric and Oceanic Technology*, 18(4), 691–703.
- 1042 Webster, P. J., Moore, A. M., Loschnigg, J. P., & Leben, R. R. (1999). Coupled ocean–
1043 atmosphere dynamics in the Indian Ocean during 1997–98. *Nature*, 401(6751), 356.
- 1044 Xavier, P. K., Marzin, C., & Goswami, B. (2007). An objective definition of the Indian
1045 summer monsoon season and a new perspective on the ENSO–monsoon relationship.
1046 *Quarterly Journal of the Royal Meteorological Society*, 133(624), 749–764.
- 1047 Yoon, J.-H., & Chen, T.-C. (2005). Water vapor budget of the Indian monsoon depression.
1048 *Tellus A*, 57(5), 770–782.
- 1049 Zarzycki, C. M., Thatcher, D. R., & Jablonowski, C. (2017). Objective tropical cyclone
1050 extratropical transition detection in high-resolution reanalysis and climate model data.
1051 *Journal of Advances in Modeling Earth Systems*, 9(1), 130–148.
- 1052 Zarzycki, C. M., & Ullrich, P. A. (2017). Assessing sensitivities in algorithmic detection of
1053 tropical cyclones in climate data. *Geophysical Research Letters*, 44(2), 1141–1149.

Supporting Information for “Assessing historical variability of South Asian monsoon lows and depressions with an optimized tracking algorithm”

S. Vishnu¹, W. R. Boos^{1,2}, P. A. Ullrich³, T. A. O’Brien^{4,2}

¹Department of Earth and Planetary Science, University of California, Berkeley, Berkeley, California, USA

²Climate and Ecosystem Sciences Division, Lawrence Berkeley National Laboratory, Berkeley, California, USA

³Department of Land, Air, and Water Resources, University of California, Davis, Davis, California, USA

⁴Earth and Atmospheric Sciences Department, Indiana University, Bloomington, Indiana, USA

Contents of this file

1. Tables S1
 2. Figures S1 to S5
-

Table S1.

LPS tracking algorithms ranked by the combined CSI. The top five algorithms and the best algorithm for each candidate search variable are given.

Rank	Variable	CCM	Radius	RH850	<i>CSI_{combined}</i>
1	STRF850	1.25E+06	10	85	0.7351
2	STRF850	1E+06	10	85	0.7303
3	STRF850	1.5E+06	10	85	0.7254
4	STRF850	7.5E+05	10	85	0.7236
5	STRF850	1.75E+06	10	85	0.7136
Top rank in other search variables					
32	GP850	125	10	85	0.6834
133	SLP	125	10	85	0.6029
359	VORT850	-4.0e-5	10	90	0.3848

CCM: closed contour magnitude, STRF850: streamfunction at 850 hPa, GP850: geopotential at 850hPa, SLP: mean sea level pressure, VORT850: relative vorticity at 850hPa, and RH850: relative humidity at 850 hPa.

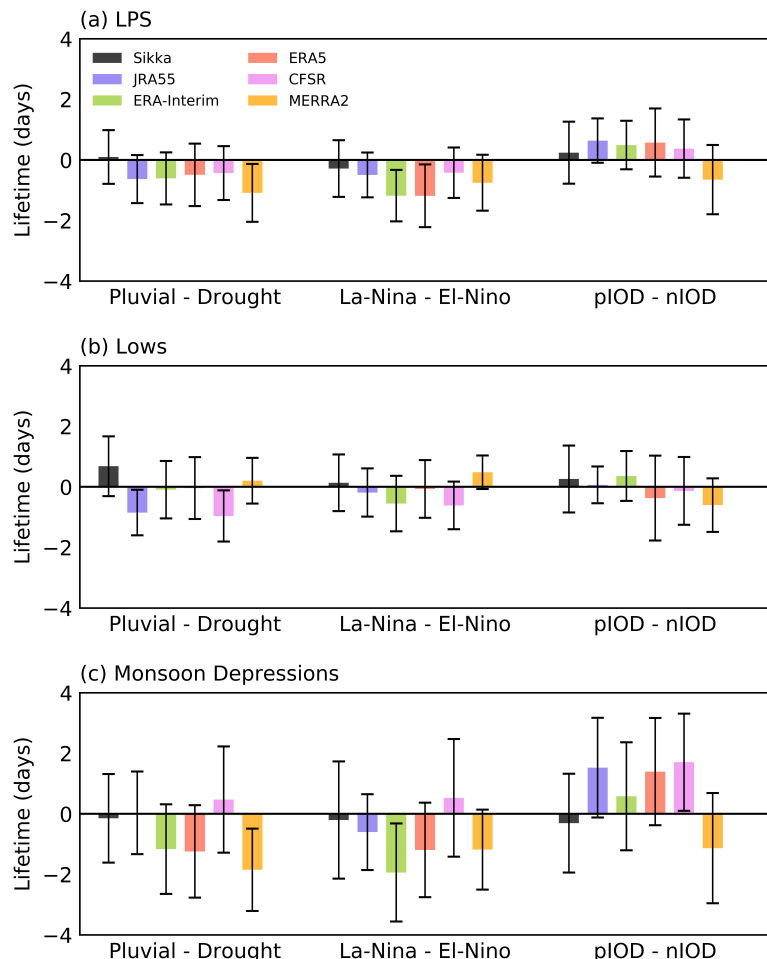


Figure S1. Difference in mean lifetime (days) of (a) LPS, (b) lows and (c) monsoon depression in pluvial-drought summer monsoon years, La Niña-El Niño and positive-negative Indian Ocean Dipole years. Vertical line represents the 95% confidence interval for the difference in the mean counts.

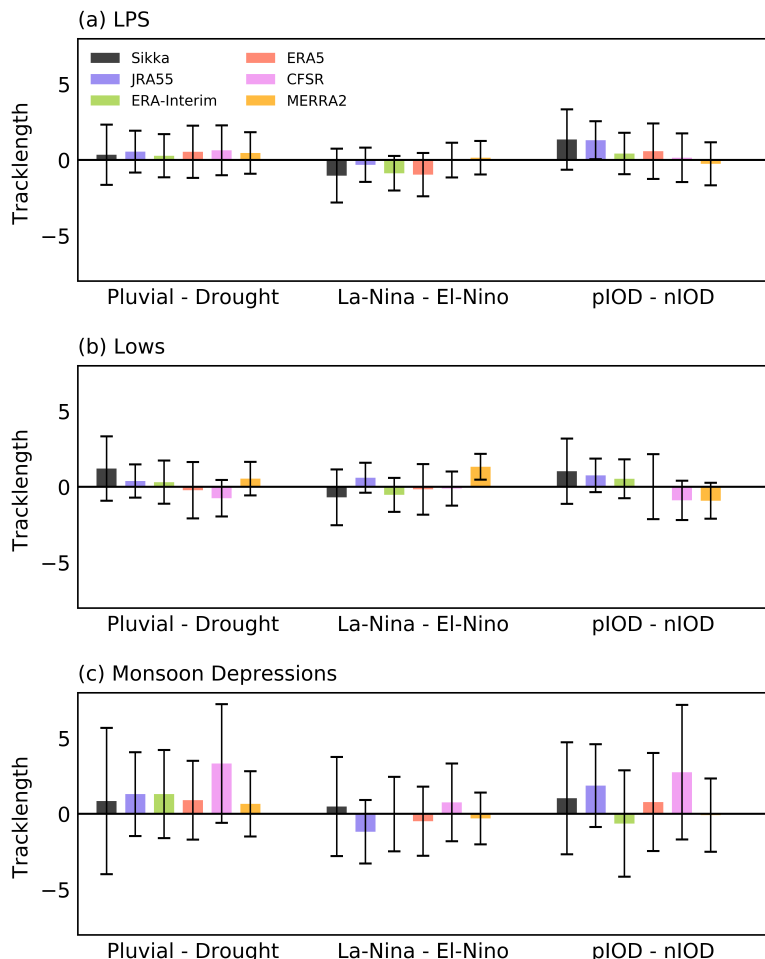


Figure S2. Difference in mean tracklength (in degrees) of (a) LPS, (b) Lows and (c) MD in pluvial-drought summer monsoon years, La Niña-El Niño and positive-negative Indian Ocean Dipole years. Vertical line represents the 95% confidence interval for the difference in the mean counts.

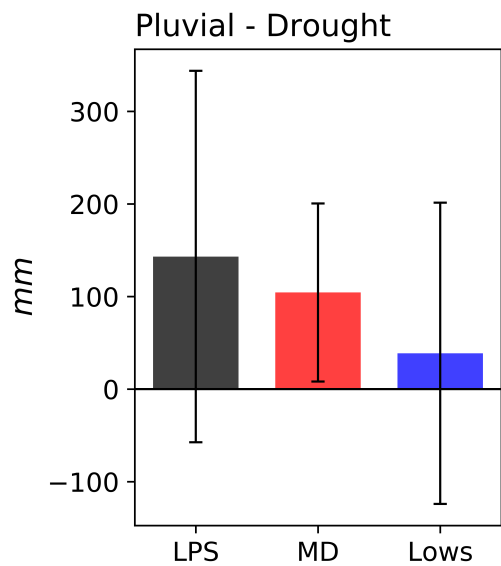


Figure S3. Difference of accumulated rainfall produced by LPS, lows and monsoon depression in pluvial-drought summer monsoon years for ERA5 dataset. Accumulated rainfall produced by the LPS in a season is the summation of averaged rainfall within the 8-degree circle of each time step when LPS is present over Indian land region. The vertical lines represent the 95% confidence interval for the difference in the mean counts.

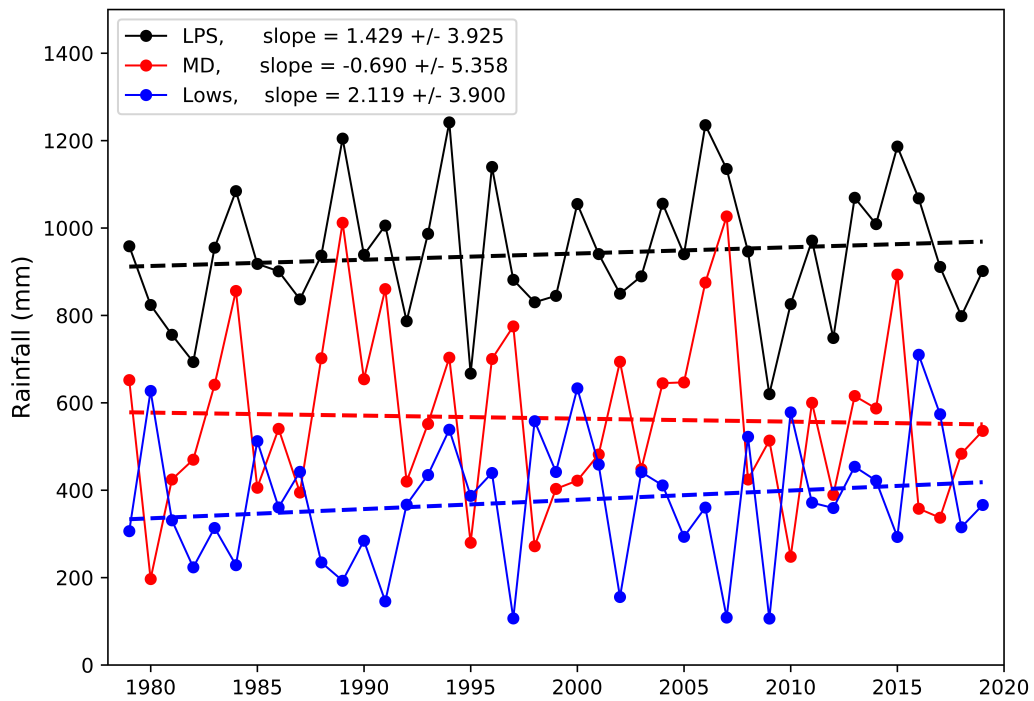


Figure S4. Linear trend of accumulated rainfall produced by LPS (black), lows (blue) and monsoon depression (red) in pluvial-drought summer monsoon years for ERA5 dataset. Accumulated rainfall produced by the LPS in a season is the summation of averaged rainfall within the 8-degree circle of each time step.

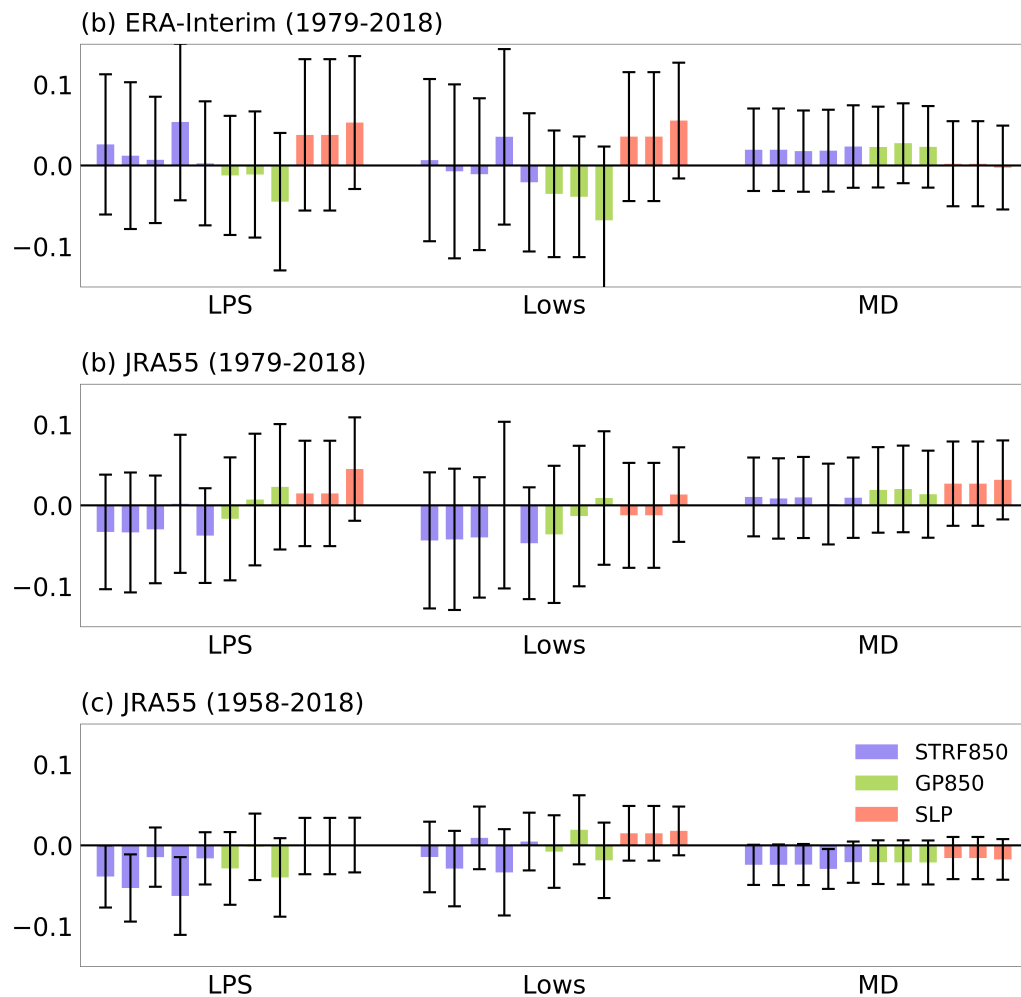


Figure S5. Linear trend in LPS, Lows and MD in (a) ERA-Interim and (b) JRA55 from 1979 onwards for top five algorithm of stream function, top three from 850 hPa geopotential and top three from SLP. Trend in JRA55 for 1958 onwards shown in (c). Error bars represent the 95% confidence interval for these trends. The 95% confidence intervals assume a normal distribution and thus are 1.96 times the standard error.